On the Macroscopic Modeling of Dilute Emulsions Under Flow

Journal:	*Journal of Fluid Mechanics*
Manuscript ID	JFM-17-S-0097.R2
mss type:	Standard
Date Submitted by the Author:	n/a
Complete List of Authors:	Mwasame, Paul; University of Delaware, Chemical and Biomolecular Engineering Wagner, Norman; University of Delaware, Chemical and Biomolecular Engineering Beris, Antony; University of Delaware, Chemical and Biomolecular Engineering
Keyword:	Emulsions < Complex Fluids, Hamiltonian theory < Mathematical Foundations, Rheology < Non-Newtonian Flows

On the Macroscopic Modeling of Dilute Emulsions Under Flow

P. Masafu Mwasame, Norman J. Wagner, Antony N. Beris[a)]

Center for Molecular and Engineering Thermodynamics,

Department of Chemical and Biomolecular Engineering, University of Delaware,

Newark, DE 19716

[a)]Corresponding Author. Tel. 1- 302- 831-8018, E-mail address: beris@udel.edu

Journal of Fluid Mechanics

Date: 8/3/2017

A new macroscopic model describing the rheology and microstructure of dilute emulsions with droplet morphology is developed based on an internal contravariant conformation tensor variable which is physically identified with the deformed ellipsoidal geometry of the dispersed phase. The model is consistent with existing first order Capillary number, $O(Ca)$, theory describing the microstructure as well as $O(Ca^2)$ theory describing the emulsion contributed extra stress. These asymptotic solutions are also used to determine all the model parameters, making it the only macroscopic emulsion model that is consistent with all available asymptotic theories in the limit of small Ca numbers. The governing equations are obtained from the Poisson and dissipation brackets, as developed for an incompressible fluid system endowed with an internal contravariant second order tensor, subject to the imposition of the constraint of a unit determinant. First proposed by Maffettone and Minale (J. Non-Newtonian Fluid Mech., vol. 78, 1998, 227), this constraint physically corresponds to the conservation of the volume of the dispersed phase in the emulsion. The Hamiltonian of the emulsion is expressed through the surface energy of the dispersed phase, in addition to the kinetic energy, following previous work by Grmela et al. (J. Non-Newtonian Fluid Mech., vol. 212, 2014, 1), but employing a more accurate evaluation of the surface area in terms of the internal contravariant conformation tensor. Structural predictions of the ellipsoid droplet morphology obtained with the new model are compared against classic experiments by Torza et al. (J. Colloid Interf. Sci. vol. 38, 1972, 395) showing good agreement.

1. Introduction

The dynamics and rheology of complex mixtures of immiscible fluids is an important area of study owing to the significance of multiphase flows in numerous industrial processes. Moreover, deformable ellipsoids are a common abstraction used to model the dispersed phase microstructure in flowing soft matter systems including emulsions (Vermant *et al.* 1998) and polymers and polymer blends (Lee & Park 1994). Rallison (1980) and Stone (1994) have extensively discussed and reviewed the subject of drop deformation from theoretical and experimental perspectives. Furthermore, numerous models, at different levels of complexity, have been proposed to capture various aspects of droplet behavior in viscous flows.

The most important advances in modeling the rheology of suspensions have been realized by connecting the microscopic analysis of the detailed flow field around the suspended particles to the macroscopic rheology of the suspension (Einstein 1906, 1911). This pioneering work by Einstein in the dilute limit of solid particle suspensions has been extended to describe higher order concentration effects and/or droplet particles with finite internal viscosity (Taylor 1932, 1934; Batchelor 1970; Happel and Brenner 1983). However, even for dilute suspensions, there are higher order effects that give rise to normal stress contributions (Schowalter, Chaffey & Brenner 1968; Frankel & Acrivos 1970; Raja, Subramanian & Koch 2010), which therefore cannot be described by a modified viscosity corresponding to a generalized Newtonian model. Moreover, for suspensions of deformable liquid particles, i.e. emulsions, the macroscopic flow induces anisotropy in the shape of the emulsion droplet as well as in the neighbor distribution. Therefore, in addition to the rheology, one has to also describe the flow-induced anisotropic microstructure. This work shows how one can take advantage of the shape anisotropy that emerges naturally as a characteristic of the system at the microscopic level to describe the overall rheological behavior at the macroscopic level in dilute emulsion suspensions. To connect the microscopic and macroscopic levels in emulsions with ellipsoidal morphology, an internal second order conformation tensor that describes the deformed ellipsoidal shape of individual droplets is used in this work**.** Following guidelines from Non-Equilibrium thermodynamics, we develop an evolution equation for the ellipsoidal droplet as well as an expression for the extra stress tensor which emulates those arising from independent asymptotic results from microscopic theory (Schowalter, Chaffey & Brenner 1968; Frankel & Acrivos 1970) in the limit of dilute emulsions.

Some of the earliest studies, on the micromechanics of single droplets in viscometric flows, were carried out by Taylor (1932, 1934), Oldroyd (1953) and Batchelor (1970). Soon thereafter, these ideas were extended to multiple droplets in viscous flows by Choi & Schowalter (1972), Palierne (1990) and

Delaby, Muller & Ernst (1995). However, since these analytical calculations, as well as corresponding numerical simulations (Rallison & Acrivos 1978; Rallison 1984; Lowenberg & Hinch 1996), are often too involved to be used directly in engineering applications, the need for more coarse-grained modeling approaches is apparent. At the coarse-grained level of modeling either covariant or contravariant tensors are used as internal variables to describe the internal microstructure depending on the morphology of interest (Minale 2010). Mathematically, these two descriptions are related through an inverse, as the inverse of the covariant tensor is a contravariant tensor and vice versa (Edwards & Dressler 2003). Nevertheless, such a one-to-one relationship should not be considered to mean that there is necessarily a one-to-one correspondence between the tensor descriptions. The validity of the inverse relationship also depends on the physical interpretations and definitions of the tensors at hand. To date, the modeling of interfaces in emulsions has been carried out primarily either through *interface* or *area tensors* (which are covariant tensor objects) or alternatively through *ellipsoid morphology tensors* (which can be cast as either covariant or contravariant tensor objects).

The interfacial tensor (Doi & Ohta 1991; Wetzel & Tucker 1999; Almusallam, Larson & Solomon 2000) is a second order tensor object that is related to the second moment of the interface density function, whose primary variable is the unit vector normal to the interface. Physically, the interfacial tensor represents the average size and orientation of the interface. In this approach, the surface area of the interface is proportional to the first invariant of the area tensor and can be computed exactly. On the other hand, the volume of the dispersed phase enclosed by the interface is difficult to calculate, and approximate relationships and/or closure rules must be used (Doi & Ohta 1991; Almusallam, Larson & Solomon 2000, 2004; Edwards & Dressler 2002; Wetzel & Tucker 1999). As a consequence, volume conservation is difficult to enforce in modeling incompressible fluids enclosed by an interface. Such models have been widely studied (Takahashi *et al.* 1994; Guenther & Baird 1996; Vinkier, Moldenaers & Mewis 1996) as constitutive equations can be developed based on the stress tensor of Batchelor (1970) which admits an interface tensor. A review of this class of models is presented by Almusallam, Larson & Solomon (2004) and Minale (2010). However, because of the above-mentioned difficulties in implementing the volume conservation constraint, we choose not to use this internal tensor variable any further within the present work.

Instead, of primary interest for this work are conformation tensor models that use the geometrical deformation of an initially spherical droplet to describe emulsion morphology. These ellipsoid morphology tensors can be categorized as either contravariant (Maffettone & Minale 1998) or covariant (Wetzel & Tucker 2001), with these two forms being both mathematically and physically equivalent. Moreover, it

should be noted that ellipsoid morphology tensors can be related to the interfacial tensor but the relationship is not one-to-one (Wetzel & Tucker 1999). In both contravariant and covariant cases, the eigenvectors of the ellipsoidal tensor are along the direction of the principle axes of the ellipsoid. However, in the contravariant tensor, the eigenvalues are proportional to the square of the semi-axes of the ellipsoid, while in the covariant they are inversely proportional. Therefore, the covariant tensor is formally the inverse of the contravariant one. In either tensor description, a connection can be made between the canonical form of an ellipsoid equation, $x^2/L^2 + y^2/B^2 + z^2/W^2 = 1$ (where *L*, *B* and *W* are the ellipsoid semi-axes and *x*, *y* and *z* coordinates on the ellipsoid surface) and the quadratic forms $\underline{\underline{C}} : \underline{q}\underline{q} = 1$ and $\underline{\underline{C}}^{-1} : \underline{q}\underline{q} = 1$ (where the vector $q = [x\ y\ z]^T$) for the covariant and contravariant forms respectively. As a result, the volume of an emulsion droplet is related to the third invariant (i.e. the determinant) of the conformation tensor and volume conservation can be strictly enforced by requiring that the third invariant is constant. In contrast, in this formulation, it is the surface area that is difficult to calculate, necessitating the use of approximate relationships, as analytical expressions only exist for specialized ellipses. Covariant (Yu & Bousima 2002; Jackson & Tucker 2003; Yu & Zhou 2007) and contravariant (Minale 2004) ellipsoid morphology tensors models have found particular success in describing experimentally observed droplet morphology in the vicinity of overcritical Capillary numbers.

The models mentioned so far are highly phenomenological. Significant advances can be made by employing a Non-Equilibrium Thermodynamics (NET) framework that combines in a systematic and consistent fashion, Hamiltonian mechanics and dissipation (Grmela 1991, 1993). In this framework, the reversible dynamics are developed based on a Poisson Bracket description of Hamiltonian Mechanics. The challenge lies in prescribing the irreversible dynamics that give rise to the dissipation. Beris & Edwards (1994) systematically described the single generator approach in which the irreversible dynamics are also generated from the system Hamiltonian through a dissipation Bracket and demonstrated its applicability towards describing classical viscoelasticity. Moving beyond this, The General Equation for Reversible and Irreversible Coupling (GENERIC), developed by Grmela & Öttinger (1997) and Öttinger & Grmela (1997), allows for the generation of reversible and irreversible dynamics based on the Hamiltonian and Entropy functionals, respectively. A detailed comparison of these developments that shows their equivalence as far as macroscopic modeling is concerned is provided by Edwards (1998) and Edwards Beris & Öttinger (1998). Several authors (Grmela & Ait-Kadi 1998; Grmela, Ait-Kadi & Utracki 1998; Wagner, Öttinger & Edwards 1999; Wagner et al. 1999) have analyzed the Doi-Ohta model from a thermodynamics perspective using the GENERIC formalism. They concluded that the dynamical equations proposed in the

Doi-Ohta model are thermodynamically consistent. Although attempts have been made at developing interfacial tensor models for ellipsoidal droplet morphologies (Almusallam, Larson & Solomon 2000, 2004; Edwards & Dressler 2002), the volume constraint is much more difficult to implement under these conditions than in the ellipsoid morphology tensor approach. This further motivates our efforts in the present work to develop a thermodynamically consistent ellipsoidal morphology tensor model.

Some previous work has already been devoted towards understanding the thermodynamic validity of ellipsoid morphology tensor model equations. Ait-Kadi *et al.* (1999) outlined the GENERIC development of a contravariant tensor model subject to a constant determinant constraint. However, this model was presented in an abstract fashion with the conformation tensor not identified with any specific microstructure, the free energy density provided as a general function of the conformation tensor invariants, and with no affine deformation. Thus, it has no direct applicability as a contravariant emulsion morphology model. Building further upon this work, Grmela, Bousima & Palierne (2001) introduced a non-affine contribution to the convected time derivative and, among other things, showed how formally a conformation-based evolution equation that resembles that of Maffettone & Minale (1998) model can be realized within the GENERIC framework for a specific form of the free energy expression. However, the conformation tensor they chose was different from that appearing in the Maffettone & Minale (1998) model in that although it also corresponds to a symmetric second order tensor whose eigenvectors are the axes of the ellipsoidal droplet, they chose the lengths of the semi-axes of the ellipsoid as its eigenvalues (as it emerges from the expression offered for the total volume V_B of the dispersed fluid (B) as $nV\det\left(\underline{\underline{b}}\right)$ where n is the droplet number density, V the total volume and $\underline{\underline{b}}$ the conformation tensor that they used). Consequently, $\underline{\underline{b}}$ is the square root of the conformation tensor $\underline{\underline{C}}$ that appears in Maffettone & Minale (1998) and if the latter (as we will show later below) is indeed a contravariant tensor, the first one is not and in consequence it is not suitable to be used as a primitive tensor variable as its reversible part does not transform either as contravariant or covariant tensor (the only two objective tensors for which a Poission bracket is available). In addition, the free energy expression that Grmela Bousima & Palierne (2001) used was arbitrary and not consistent with the expected form of the surface free energy when expressed in terms of the conformation tensor necessitating further improvements.

Subsequently, Grmela *et al.* (2014), advanced a free energy expression specifically to express the surface energy of the droplets. In this free energy expression the surface area was identified with the second invariant of the conformation tensor, which is a reasonable but significant approximation. Despite this improvement, the main problem with the latest Grmela *et al.* (2014) model is that the conformation

tensor used is, like $\underline{\underline{b}}$ before, identified with square root of the Maffettone & Minale (1998) contravariant conformation tensor, and therefore this is not a contravariant tensor. A further corroborative proof that this is the meaning of the second order tensor used by Grmela *et al.* (2014) is that it has units of length, leading to a second invariant with units of length squared, therefore making the second invariant suitable to represent the ellipsoid surface as they did. As a consequence, if the correct physics of the Maffettone & Minale (1998) physical picture is to be followed, it is the square of the tensor used by Grmela *et al.* (2014) that is contravariant and for which a relevant Poisson bracket can be built to represent its reversible dynamics; treating its square root as the contravariant tensor object following Grmela *et al.* (2014) makes the developed model equations inconsistent with the physics of emulsion deformation. Still, the model equations developed in Grmela *et al.* (2014) can be used but need to be considered as phenomenological approximations of the underlying physics of droplet deformation dynamics.

Therefore, the need for a physically-based and thermodynamically consistent emulsion morphology-based contravariant tensor model still remains. Thermodynamic consistency is important because through it one avoids unnatural model instabilities and/or aphysical results corresponding to a negative rate of entropy production (Beris & Edwards 1994). It also guarantees physical results for general flows, not just simple shear flow. In addition, it highlights the intimate connection between the conformation tensor and the stress tensor which underlies the rheological response that is absent in phenomenological models like the MM model (Maffettone & Minale 1998). In these models, the only way to obtain the deformed droplet-induced stress is by using the stress expression of Batchelor (1970). However, this limits the use of these models for equal the disperse and continuous phase viscosities because if they are different the interfacial velocity (which is not accessible through a phenomenological model) is needed. To move beyond current model capabilities, a Thermodynamically Consistent Ellipsoidal Emulsion (TCEE) model is systematically developed in the present work, and validated by showing its consistency against known independent microscopic asymptotic theories in the limit of small Capillary numbers. In parallel, the results from asymptotic theory are used to a-priori determine all parameters of the TCEE model thus allowing for the realization of a purely predictive macroscopic model.

The key essence of this work is to demonstrate that it is possible to construct a macroscopic theory for dilute emulsion flow that is consistent with known microscopic results for both the microstructure and the stress tensor. In this way, the number of adjustable parameters is significantly reduced. Furthermore, moving beyond traditional phenomenological models (such as Maffettone & Minale (1998) and Wetzel & Tucker (2001)) that place an emphasis on only describing droplet deformation and orientation, the present work introduces a systematic approach towards developing corresponding expressions for the

stresses consistent with both the droplet microstructure and available theoretical microscopic results. In this way, this work distinguishes itself even from related thermodynamically consistent emulsion flow models in the literature (Grmela *et al.* 2014). A word needs to be said that although the present work restricts itself to the (usual in material constitutive equations) particle inertialess limit, the thermodynamic approach followed can also be generalized to include particle inertia effects (characterized by the particle Reynolds number), as addressed in a subsequent publication (Mwasame, Wagner & Beris 2017). Furthermore, we need to stress that in order to keep the complexity at a minimum, we opted here to offer a version of the theory with the minimum complexity necessary to match available microscopic theory to $O(1)$ in the conformation tensor evaluation and $O(Ca^2)$ in the stress. However, if so needed, the approach we present can be extended, at the expense of additional complexity, to also accommodate additional information from asymptotic theory and/or experimental results, while still preserving the consistency with the asymptotic expression employed in this work.

In the next section we summarize two contravariant ellipsoid morphology models from the literature, the MM and MMG models, as well as asymptotic results from microscopic theory. In section 3, we first present the complete description of the Poisson and Dissipative bracket structure in the presence of a unit determinant constraint following closely the work of Edwards *et al.* (2003) as well as a description of the correct subspaces in which the Volterra derivative must be evaluated. Then, we describe the form of the surface free energy assuming an ellipsoidal droplet. Moreover, we show how the model parameters can be selected so that the TCEE model is fully compatible with existing asymptotic expansions previously developed by Schowalter, Chaffey & Brenner (1968) and also Frankel & Acrivos (1970). In section 4, the TCEE model predictions are compared against the MM model as well as against experimental data by Torza, Cox & Mason (1972). In that section, we also demonstrate the consistency of the TCEE model with theoretical results by Taylor (1934) and Chaffey & Brenner (1967) at small Capillary numbers. Finally, in section 5, we present our conclusions.

2. Previous ellipsoid morphology models and asymptotic results in the literature

This section provides a brief overview of two conformation tensor based models designed for emulsions comprised of Newtonian constituents as well as some relevant asymptotic results from microscopic investigations.

2.1. The Maffettone and Minale (MM) model

Maffettone & Minale (1998) developed a specialized and phenomenological expression, subsequently referred to as the MM model, to describe the dynamics of non-coalescing and non-breaking

ellipsoidal droplets in a general flow field. The droplet morphology is described by a contravariant second rank structural tensor $\underline{\underline{C}}$ subject to a unit determinant constraint to guarantee that the volume of the drop is conserved. This model is applicable to dilute and semi-dilute polymer blends, with ellipsoidal morphology, in which the droplet relaxation is expected to be minimally affected by hydrodynamic interactions between droplets. The validity of such an assumption is supported by literature results (Vinkier, Moldenaers & Mewis 1996; Vinkier, Mewis & Moldenaers 1997) that show it is possible to predict the rheological response of a polymer blend when the deformation of a single droplet is known as a function of shear rate. However, unlike the Doi-Ohta model, the evolution equation for $\underline{\underline{C}}$ has no accompanying stress equation.

In the MM model, the eigenvectors and eigenvalues of $\underline{\underline{C}}$ correspond to the direction and square of the magnitude, respectively, of the dimensionless principal semi-axes of the ellipsoidal droplet, the lengths of the semi-axes made dimensionless using the equilibrium droplet radius. As a result of the nondimensionalization, we can express the volume constraint resulting from the mass preservation of a droplet (assumed incompressible and that no breakage or coalescence takes place) by taking the determinant of $\underline{\underline{C}}$ (which is proportional to the square of the volume of the ellipsoidal droplet that it represents given its definition above) constant and equal to unity: $I_3 \equiv \det\left(\underline{\underline{C}}\right) = 1$. The relaxation mechanism for the droplet dynamics is then provided by the surface tension which acts to return the deformed ellipsoid to a spherical shape.

The dynamical equation for the conformation tensor variable provided by Maffettone and Minale (1998) is

$$\frac{D\underline{\underline{C}}}{dt} - \left(\underline{\underline{\Omega}} \cdot \underline{\underline{C}} - \underline{\underline{C}} \cdot \underline{\underline{\Omega}}\right) + \left(\xi - 1\right)\left(\underline{\underline{D}} \cdot \underline{\underline{C}} + \underline{\underline{C}} \cdot \underline{\underline{D}}\right) = -\frac{1}{\tau}\left(\underline{\underline{C}} - \frac{3}{I_2}\underline{\underline{\delta}}\right) . \tag{1}$$

The left hand side of Eq. (1) is the Gordon-Schowalter time derivative defined in terms of the rate of strain ($\underline{\underline{D}}$) and vorticity tensors ($\underline{\underline{\Omega}}$) and the dimensionless non-affine parameter ξ. The rate of strain tensor, $\underline{\underline{D}}$, is defined as

$$\underline{\underline{D}} = \frac{1}{2}\left(\left(\underline{\nabla V}\right)^T + \left(\underline{\nabla V}\right)\right) , \tag{2}$$

while the vorticity tensor, $\underline{\underline{\Omega}}$, is defined as

$$\underline{\underline{\Omega}} = \frac{1}{2}\left(\left(\underline{\nabla V}\right)^T - \left(\underline{\nabla V}\right)\right) . \tag{3}$$

In addition, I_2 describes the second invariant of the conformation tensor $\underline{\underline{C}}$ defined as

$$I_2 = \frac{1}{2}\left(tr\left(\underline{\underline{C}}\right)^2 - tr\left(\underline{\underline{C}} \bullet \underline{\underline{C}}\right)\right), \tag{4}$$

where $tr(\ )$ is the trace, and $tr\left(\underline{\underline{C}}\right)$ represents the first invariant, I_1, of $\underline{\underline{C}}$. Finally, in Eq. (1), τ represents a characteristic relaxation time. Note that the constraint $I_3 = \det\left(\underline{\underline{C}}\right) = 1$ once satisfied by the initial conditions is duly preserved by the dynamics described by Eq. (1).

The parameters ξ and τ in Eq. (1) can now be expressed in terms of the original symbols employed by Maffettone & Minale (1998). The relaxation time τ entering Eq. (1) is defined in terms of the original parameters as $\tau \equiv \tau_C / f_1$, where τ_C is a characteristic time defined as $\tau_C \equiv \mu a / \gamma$, with γ the surface tension, μ the continuous phase viscosity and a is the equilibrium radius of the emulsion droplet, while $f_1 = 40(\lambda+1)/\left((19\lambda+16)(2\lambda+3)\right)$ is assumed to be a function of the viscosity ratio, λ, where $\lambda \equiv \mu_d / \mu$ and μ_d is the dispersed phase viscosity. Finally, $\xi = 1 - f_2$, where $f_2 = 5/(2\lambda+3)$, and takes values ranging from 0 to 5/3.

A key observation from the MM model is that the time derivative used for the $\underline{\underline{C}}$ tensor, as expressed by the left-hand-side of Eq. (1), is the Gordon-Schowalter time derivative (Gordon & Showalter 1972). A value of $\xi = 1$ is the limit of full non-affine motion and the left-hand-side of Eq. (1) reduces to the Jaumann derivative (Jaumann 1911). On the other hand, a value $\xi = 0$ corresponds to fully affine motion, and the left-hand-side of Eq. (1) reduces to the upper-convected time derivative. Moving forward, the Gordon-Schowalter time derivative will be denoted by the following shorthand

$$\frac{D^{(\xi)}\underline{\underline{C}}}{dt} \equiv \frac{D\underline{\underline{C}}}{dt} - \left(\underline{\underline{\Omega}} \cdot \underline{\underline{C}} - \underline{\underline{C}} \cdot \underline{\underline{\Omega}}\right) + (\xi - 1)\left(\underline{\underline{D}} \cdot \underline{\underline{C}} + \underline{\underline{C}} \cdot \underline{\underline{D}}\right) . \tag{5}$$

The next observation is that the relaxation term in the MM model incorporates a non-linear dependence on the second invariant. We note that Eq. (1) may be considered to be phenomenological and does not by itself allow one to obtain an expression for a rigorous stress tensor except in the very specific limit of $\lambda = 1$ where Batchelor's stress formula can be used (Batchelor 1970). This is the one of the motivations for the development of a recent model described by Grmela *et al.* (2014), which is described next.

2.2. The MMG model

Applying a thermodynamically consistent methodology to a contravariant internal conformation tensor, Grmela *et al.* (2014) derived a macroscopic phenomenological approximation of the MM model, referred to here as the MMG model. This model is applicable to isothermal emulsions and also includes

an extension towards describing emulsions with non-ellipsoidal shapes. The main advantage of the Grmela *et al.* (2014) approach is that starting from an expression for the free energy, H, a constitutive equation for the stress tensor is also derived consistently from the Non-Equilibrium Thermodynamics formalism. Their free energy expression, in terms of a dimensional conformation tensor, was specified by

$$H = \int \left(\frac{\underline{\underline{u}}^2}{\rho} + \overline{\Gamma}\chi \left(tr\left(\underline{\underline{\overline{C}}}\right)^2 - tr\left(\underline{\underline{\overline{C}}}\,\underline{\underline{\overline{C}}}\right) \right) - k_B \mathrm{T}\chi \ln\det\left(\underline{\underline{\overline{C}}}\right) \right) d^3r \,. \tag{6}$$

where the terms on the right-hand side are the kinetic energy density, surface energy density and entropy density, respectively. In this expression, $\underline{u}$ is the momentum density, $\underline{\underline{\overline{C}}}$ is identified as a dimensional contravariant internal conformation tensor[1] with units of length, ρ is the mass density, χ is the number density, $\overline{\Gamma}$ is the surface tension (energy per area) and $k_B\mathrm{T}$ is the thermal energy (energy per molecule). Since $\left(tr\left(\underline{\underline{\overline{C}}}\right)^2 - tr\left(\underline{\underline{\overline{C}}}\,\underline{\underline{\overline{C}}}\right) \right)$ is considered a measure of the area of the ellipsoid, with units of length squared (consistent to the previously mentioned units of length for $\underline{\underline{\overline{C}}}$), we use here the product $\overline{\Gamma}\chi$ as its weight instead of a composite parameter Γ (as it appeared in the original Grmela *et al.* (2014) work) to separate the dependence on the number density and allow for the consideration of as $\overline{\Gamma}$ the surface tension. Furthermore, if $\underline{\underline{\overline{C}}}$ is made dimensionless by dividing it by a characteristic length resulting in a dimensionless conformation tensor $\underline{\underline{C}}$, $\underline{\underline{C}} \equiv \underline{\underline{\overline{C}}} / \ell$, the free energy expression becomes

$$H = \int \left(\frac{\underline{\underline{u}}^2}{\rho} + 2\Gamma\chi I_2 - k_B \mathrm{T}\chi \ln\det\left(\underline{\underline{C}}\right) \right) d^3r \,, \tag{7}$$

with $\Gamma \equiv 4\pi\ell^2\overline{\Gamma}$ now interpreted as the surface energy of an undeformed drop of radius ℓ and I_2 the second invariant of $\underline{\underline{C}}$ that accounts for the effect of surface deformation. This expression, with correct units, is the one to be used here in lieu of that originally presented by Grmela *et al.* (2014) to facilitate the comparison between this model, the MM model and, eventually, the TCEE model presented in this work.

Similar to the MM model, the time derivative in the MMG model is the standard Gordon-Schowalter time derivative. Additionally, the relaxation term is developed based on a dissipative potential. At the end, the evolution equation of the dimensional conformation tensor $\underline{\underline{C}}$ that describes the microstructure in the MMG model can be represented as (Grmela *et al.* 2014)

[1] Note that in the discussion on the MMG model presented in Grmela *et al.* (2014), the conformation tensor used as the structural variable is referred to as the Hand tensor (Hand 1962).

$$\frac{D^{(\xi)}\underline{\underline{C}}}{dt} = -\left(\frac{1}{2}\left(\underline{\underline{\Lambda}}\,\underline{\underline{X}} + \underline{\underline{X}}\,\underline{\underline{\Lambda}}\right) - \frac{1}{3}tr\left(\underline{\underline{\Lambda}}\,\underline{\underline{X}}\,\underline{\underline{\hat{C}}}^{-1}\right)\underline{\underline{C}}\right) - \frac{2}{3}\underline{\underline{C}}\left(tr\left(\left(\underline{\nabla V}\right)\right) - \xi tr\left(\underline{\underline{D}}\right)\right), \tag{8}$$

where

$$\begin{aligned} \underline{\underline{\Lambda}} &= \Lambda\underline{\underline{C}} \\ \underline{\underline{X}} &= \underline{\underline{C}}^{*} - \frac{1}{3}tr\left(\underline{\underline{C}}\,\underline{\underline{C}}^{*}\right)\underline{\underline{C}}^{-1}, \end{aligned} \tag{9}$$

and $\underline{\underline{C}}^{*}$, the Volterra derivative of the free energy with respect to the conformation tensor $\underline{\underline{C}}$, is given by

$$\underline{\underline{C}}^{*} \equiv \frac{\delta\Phi}{\delta\underline{\underline{C}}} = 2\chi\Gamma tr\left(\underline{\underline{C}}\right)\underline{\underline{\delta}} - 2\chi\Gamma\underline{\underline{C}} - \frac{4}{3}\chi\Gamma I_2\underline{\underline{C}}^{-1}\,^{2}. \tag{10}$$

The inner structure of the MMG model can be further elucidated by simplifying Eq. (8), through the use of Eqs. (9) and (10), to

$$\frac{D^{(\xi)}\underline{\underline{C}}}{dt} = -\frac{1}{\tau_{MMG}}\left(\left(\frac{I_1}{2} + \frac{I_2^2}{3}\right)\underline{\underline{C}} - \frac{3}{2}\underline{\underline{C}}\,\underline{\underline{C}} - I_2\underline{\underline{\delta}}\right) - \frac{2}{3}\underline{\underline{C}}\left(tr\left(\left(\underline{\nabla V}\right)\right) - \xi tr\left(\underline{\underline{D}}\right)\right), \tag{11}$$

where, τ_{MMG} is a single material parameter with the units of time defined as $\tau_{MMG} \equiv \left(4\chi\Gamma\Lambda/3\right)^{-1}$. The left-hand side of Eq. (11) reflects the reversible convective effects. On the other hand, the first term on the right hand side of Eq. (11) is the relaxation while the second term is a correction to the reversible dynamics arising from the implementation of the volume constraint. For incompressible simple shear flows, the last term does not contribute to the evolution of the conformation tensor as $tr\left(\underline{\nabla V}\right) = tr\left(\underline{\underline{D}}\right) = 0$. Such a term is absent in the MM model, indicating an inherent limitation of its application, as written, only to flow fields with a traceless divergence-free rate of strain tensor. Finally, the interfacial stress contribution is computed in the MMG model, self-consistently, based on the free energy expression indicated in Eq. (7) as

$$\underline{\underline{\sigma}} = 4\chi\Gamma\left(1-\xi\right)\left(I_{\underline{\underline{C}}}\underline{\underline{C}} - \underline{\underline{C}}\cdot\underline{\underline{C}} - \frac{2}{3}II_{\underline{\underline{C}}}\underline{\underline{\delta}}\right). \tag{12}$$

[2] Note this expression for the Volterra derivative differs from that appearing in Grmela et al. (2014), which did not properly account for the volume constraint when evaluating Volterra derivatives (see Appendix A).

Variables / Parameters	Units	Description
$\underline{\underline{C}}$	-	Shape and size tensor
$k_B \mathrm{T}$	E	Thermal energy
Γ	E	Surface energy
χ	L^{-3}	Number density
Λ	$\mathrm{L}^3 \mathrm{T}^{-1} \mathrm{E}^{-1}$	Relaxation pre-factor

TABLE 1. Summary of dimensional parameters entering the model: E=energy, L=length and T=time.

The final set of parameters entering the MMG model (Eqs. (6), (11) and (12)) are succinctly denoted by the vector $P_{MMG} = [\xi, \chi, \Gamma, \Lambda]$. Table 1 presents the various dimensions associated with the conformation tensor and the four parameters appearing in the model. Note that in the final equations (Eqs. (11) and (12)), only 3 of these are truly independent: τ_{MMG}, ξ and the product $\chi\Gamma$. The free energy expression in Eq. (6), through the surface energy term, identifies the surface area with the second invariant of the conformation tensor. As noted before, in comparing the MMG model to the MM model, the main issue with the MMG model is that its conformation tensor is physically identified with the square root of the contravariant tensor describing an ellipsoid and therefore its reversible dynamics cannot be described by a Poisson structure. Therefore, we consider this model both phenomenological and thermodynamically inconsistent in the context of $\underline{\underline{C}}$ representing an ellipsoid.

From a mathematical point of view, comparing Eq. (11) to Eq. (1) also reveals other differences between the two models. Although both models incorporate a non-linear relaxation term that depends on the invariants, the MMG model possesses an additional non-linear term proportional to $\underline{\underline{C}}\,\underline{\underline{C}}$. There are also similarities between the two models. First, in both models, the dimensionless conformation tensor, $\underline{\underline{C}}$, is subject to the constraint $I_3 = 1$ which means the equilibrium state is identified with $\underline{\underline{C}} = \underline{\underline{\delta}}$. Second, it is clear that the evolution equations for the conformation tensor in both models have 2 macroscopic parameters, ξ and τ, the first dimensionless and the second with units of time, respectively. An additional benefit of the Non-Equilibrium Thermodynamics framework underlying the MMG model is the stress tensor that arises self-consistently, a feature absent in the original phenomenological MM model.

The discussion so far has revealed important limitations in both the MM and MMG model, providing justification for the development of improved ellipsoid morphology models. Furthermore, since we seek to describe the general development of a Thermodynamically Consistent Ellipsoidal Emulsion (TCEE) model, with the key novelty being the exploitation of previous asymptotic results for suspension stress, these are first described before we move on to discuss the development of a TCEE model.

2.3. Asymptotic results from the literature

Microscopic calculations by Showalter, Chaffey & Brenner (1968) and Frankel & Acrivos (1970), for the rheology of dilute emulsion drops in the absence of inertia, provide the asymptotic results for the effect of drop deformation on the rheology. Drop deformation leads to non-Newtonian rheology at large Capillary numbers (Ca), where $Ca \equiv \mu a\dot{\gamma}/T$, and to $O\left(\left(Ca^*\right)^2\right)$ (where $Ca^* \equiv \mu a/T$ is the interfacial relaxation time) the stress in such an emulsion in a linear flow field is given by the results of Showalter et al. (1968) as

$$\underline{\underline{\sigma}} = 2\mu\left(1+\phi\left(\frac{5\lambda+2}{2\left(\lambda+1\right)}\right)\right)\underline{\underline{D}} - \phi Ca^*\mu\left\{\begin{array}{l}\frac{1}{40}\left(\frac{19\lambda+16}{\lambda+1}\right)^2\left(\frac{D}{Dt}\underline{\underline{D}} - \left(\underline{\underline{\Omega}}\cdot\underline{\underline{D}} - \underline{\underline{D}}\cdot\underline{\underline{\Omega}}\right)\right) \\ -\frac{3\left(19\lambda+16\right)\left(25\lambda^2+41\lambda+4\right)}{140\left(\lambda+1\right)^3}\left(\underline{\underline{D}}\cdot\underline{\underline{D}} - \frac{1}{3}tr\left(\underline{\underline{D}}\cdot\underline{\underline{D}}\right)\underline{\underline{I}}\right)\end{array}\right\} + O(Ca^{*2}) \quad . \tag{13}$$

The zeroth order contribution to the suspension stress is due to the presence of emulsion droplets and solely influences the effective Newtonian viscosity, as was first presented by Taylor (1932). As seen from Eq. (13), the $O(Ca^*)$ effects ultimately couple non-linearly to the imposed velocity gradient. Therefore, in addition to thermodynamic consistency, the resultant model we seek to develop should also be able to reproduce the functional dependencies present in the asymptotic solution in Eq. (13), which is derived from microscopic considerations.

3. General development of a Thermodynamically Consistent Ellipsoidal Emulsion (TCEE) model

The systematic development of a thermodynamically consistent conformation tensor-based dilute emulsion model is revisited with four main goals in mind: (1) To clarify the nature and physical interpretation of the allowed microstructural variable $\underline{\underline{C}}$ with relation to idealized, reversible dynamics, (2) To understand the role of the approximation inherent in the underlying free energy expression, (3) To understand how the macroscopic parameters entering the model equations may be evaluated while at

the same time ensuring consistency with asymptotic results provided by Eq. (13) and (4) To ensure the proper implementation of the volume conservation constraint through the determinant.

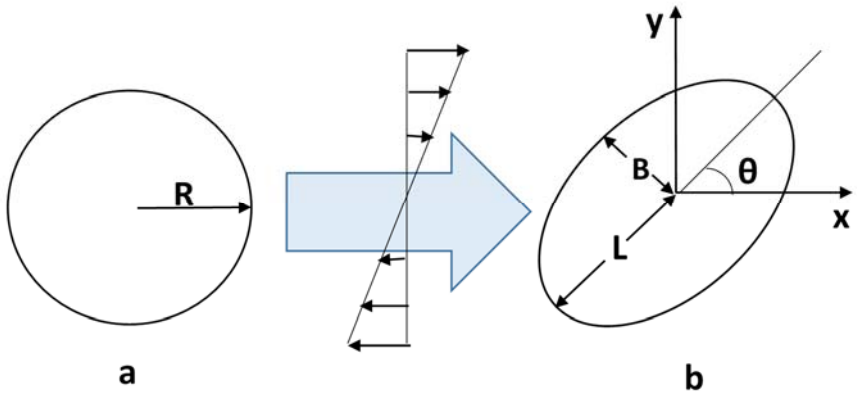

FIGURE 1: Representation of an equilibrium emulsion droplet (a) and the effect of a shear field in deforming the droplet into an ellipsoidal droplet (b), showing the various geometric parameters when projected in the x-y plane (plane of shear).

3.1. Selection of the conformation tensor variable

The development of the conformation tensor model begins by making the connection between the internal, dimensional, conformation tensor variable, $\underline{\underline{\tilde{C}}}$, and the canonical representation of the ellipsoid shown in Fig. 1. The canonical representation of an ellipsoid is given by

$$\frac{\tilde{x}_e^2}{L^2}+\frac{\tilde{y}_e^2}{B^2}+\frac{\tilde{z}_e^2}{W^2}=1\ , \tag{14}$$

where L, B and W are the principal semi-axes of the ellipsoid and $\left[\tilde{x}_e \quad \tilde{y}_e \quad \tilde{z}_e\right]\equiv\underline{\tilde{r}}_e$ are the dimensional coordinates of a point at the surface of the ellipsoid in a coordinate system constructed along the direction of the axes of the ellipsoid from its center. Through a similarity transformation, we can express the same relationship in a general coordinate system $\left(x \quad y \quad z\right)$ in tensorial notation as

$$\tilde{C}_{ij}^{-1}\tilde{r}_i\tilde{r}_j=\underline{\tilde{r}}^T\cdot\underline{\underline{\tilde{C}}}^{-1}\cdot\underline{\tilde{r}}=1\ , \tag{15}$$

where $\underline{\tilde{r}}=[\tilde{x},\ \tilde{y},\ \tilde{z}]$ is the dimensional position vector of any point on the ellipsoid surface with $\underline{\underline{\tilde{C}}}$ identified through the similarity transformation with a second order symmetric positive definite tensor with eigenvalues and eigenvectors the square of the magnitude and the direction of the semi axes of the ellipsoid, respectively. For dimensional consistency, it follows from Eq. (15) that $\underline{\underline{\tilde{C}}}$ has units of length squared. If we now construct the corresponding dimensionless tensor $\underline{\underline{C}}$, where $\underline{\underline{C}}\equiv\frac{1}{R^2}\underline{\underline{\tilde{C}}}$ (made

dimensionless by the equilibrium droplet radius, see Fig. 1), then Eq. (15) transforms to the following equivalent quadratic form

$$\underline{r}^{T}\cdot\underline{\underline{C}}^{-1}\cdot\underline{r}=1\ , \tag{16}$$

where $\underline{r}\equiv\tilde{\underline{r}}/R$ is the dimensionless position vector of any point on the ellipsoid surface. Note that consistently we recover from Eq. (16) the equation for a unit sphere as

$$\underline{r}^{T}\cdot\underline{\underline{I}}\cdot\underline{r}=1\ , \tag{17}$$

characterizing the static (equilibrium) conditions of a droplet at zero deformation with $\underline{\underline{C}}=\underline{\underline{C}}_{equil}=\underline{\underline{I}}$ and $\underline{\underline{I}}$ the identity tensor. This interpretation of the dimensionless conformation tensor $\underline{\underline{C}}$ properly identifies it with the tensor used in the MM model by Maffettone & Minale (1998). The significance of this interpretation is that it allows us, as we show immediately below, to determine the proper tensorial nature of $\underline{\underline{C}}$ as revealed upon the application of an infinitesimal, reversible, affine material deformation thereby allowing for the selection of the correct Poisson bracket descriptor of its reversible dynamics.

From the theory of elasticity, for an ideal ellipsoid (as obtained at zero interfacial tension and for a viscosity ratio of one) that deforms affinely with the flow field, and for an infinitesimal deformation, it is the Cauchy strain tensor that provides the correct co-deformational characteristics that describe how points on the boundary of the ellipsoid move. This tensor is the product of the finger tensor with its transpose i.e. $\underline{\underline{C}}=\underline{\underline{F}}\underline{\underline{F}}^{T}$, with $F_{ij}\equiv\dfrac{\partial r_i'}{\partial r_j}$ the Finger strain tensor connecting the deformed (primed) and the initial (undeformed) spatial coordinates. As a consequence of this definition and following an infinitesimal deformation $\underline{r}\rightarrow\underline{r}'$ we have

$$\underline{r}'=\underline{\underline{F}}\cdot\underline{r};\quad\text{infinitesimal deformation}\ . \tag{18}$$

Let us now assume that we start from an initially undeformed spherical droplet, with a (dimensionless) radius of unity. Consequently every point, $\underline{r}$, of the droplet's surface obeys the previously mentioned Eq. (17), corresponding (consistently) to $\underline{\underline{C}}=\underline{\underline{C}}_{equil}=\underline{\underline{I}}$. On the other hand, upon an infinitesimal deformation $\underline{r}\rightarrow\underline{r}'$ the sphere transforms to an ellipsoidal droplet, with any point $\underline{r}'$ on its surface obeying (from Eq. (16))

$$\underline{r}'^{T}\cdot\underline{\underline{C}}^{-1}\cdot\underline{r}'=1\ ;\quad\text{deformed, ellipsoidal, droplet.} \tag{19}$$

Substitution of Eq. (18) into Eq. (19) leads to

$$\left(\underline{\underline{F}}\cdot\underline{r}\right)^{T}\cdot\underline{\underline{C}}^{-1}\cdot\left(\underline{\underline{F}}\cdot\underline{r}\right)=1\Leftrightarrow\underline{r}^{T}\cdot\underline{\underline{F}}^{T}\cdot\underline{\underline{C}}^{-1}\cdot\underline{\underline{F}}\cdot\underline{r}=1\ ;\quad\text{deformed, ellipsoidal, droplet,}\tag{20}$$

which is expressed now in terms of the position vector $\underline{r}$ of the surface of the undeformed original droplet. But anyone such point is known by definition to obey the unity sphere surface definition, Eq. (17) to which therefore Eq. (20) must be equivalent. Direct comparison of those two equations leads therefore to the equality

$$\underline{\underline{F}}^{T}\cdot\underline{\underline{C}}^{-1}\cdot\underline{\underline{F}}=\underline{\underline{I}}\Leftrightarrow\underline{\underline{F}}^{T}=\left(\underline{\underline{C}}^{-1}\cdot\underline{\underline{F}}\right)^{-1}=\underline{\underline{F}}^{-1}\cdot\underline{\underline{C}}\Leftrightarrow\underline{\underline{C}}=\underline{\underline{F}}\cdot\underline{\underline{F}}^{T}\ ,\tag{21}$$

thus making equivalent the conformation tensor $\underline{\underline{C}}$, for this infinitesimal reversible deformation to the Cauchy strain tensor, $\underline{\underline{F}}\cdot\underline{\underline{F}}^{T}$. But, as shown in Ch. 5 of (Beris and Edwards 1994), the dynamics of the Cauchy strain tensor under flow are provided by the upper-convected time derivative, consistent to the contravariant character of the Cauchy tensor. This therefore proves that the conformation tensor $\underline{\underline{C}}$ defined in this way is also contravariant and that its reversible dynamics, also described by an upper-convected derivative, can be generated by the same Poisson structure that was developed in Ch. 5 of (Beris & Edwards, 1994) for contravariant tensor dynamics.

Alternatively, in a similar fashion, we can also show that $\underline{\underline{C}}^{-1}$ is covariant in character and that its dynamics can also be described by a Poisson bracket that gives rise to the lower-convected time derivative. Note that these are the only two power forms of $\underline{\underline{C}}$, i.e. $\underline{\underline{C}}^{p}$ with $p=1$ or -1, that possess a Poisson bracket structure. For any other power law coefficient p, the dynamics of the tensor $\underline{\underline{C}}^{p}$ cannot be expressed solely in terms of the same tensor, thus precluding its direct description through a Poisson bracket, or, equivalently, its usage as a primitive internal variable within a Non-Equilibrium, bracket formulation, thermodynamics description. Furthermore, this interpretation on the nature of the primitive conformation tensor to be used to describe a deformed ellipsoidal model droplet enforces strict restrictions on the relationship between the surface area of the ellipsoid (and therefore its surface energy) and its evaluation based on the invariants or eigenvalues of $\underline{\underline{C}}$, providing further evidence why the MMG model is not thermodynamically consistent.

Once the proper tensorial character (i.e. contravariant or covariant nature) of the internal conformation tensor is identified, its Poisson bracket and therefore its reversible dynamics are also in principle fully determined. However, this is true for an unconstrained conformation tensor, as that used,

for example, in describing polymer dynamics (Beris & Edwards, 1994). In the present case, the constraint of unit determinant needs to properly be taken into account. As it turns out, this modifies all subsequent structure (i.e. both the reversible as well as the irreversible dynamics) as explained in detail in subsection 3.2 below. Once the general equations are described generically in that subsection in terms of the free energy and the dissipation bracket kernels expressions, the specific choices that we consider as most appropriate to described the flow dynamics of a dilute emulsion are presented in subsections 3.3 - 3.5 eventually enabling us to fully define the proposed model. In the last two subsections, 3.6 and 3.7, the proposed model is validated by contrasting its predictions against those independently developed through microscopic analysis around a deformable droplet in the asymptotic limit of small Capillary numbers. This comparison allows us, simultaneously to the model validation, to also determine uniquely all the model parameters.

3.2. Development of the governing equations for a constrained contravariant tensor-based model through the bracket formulation

A constant volume droplet may be described by a conformation tensor with a constant determinant, which upon suitable rescaling can be equated, for simplicity, to unity, without loss of generality. The introduction of such microstructural constraints must be implemented at the bracket level to ensure that the resulting equations are consistent with the constraints (Edwards *et al.* 2003). For completion, we repeat the essential components of such a development. Following Edwards *et al.* (2003), the appropriate transformation from an unconstrained $\underline{\underline{q}}$ tensor to a unit determinant-constrained $\underline{\underline{C}}$ tensor is given by

$$\underline{\underline{q}} \to \underline{\underline{C}} = \frac{\underline{\underline{q}}}{\left(\det\left(\underline{\underline{q}}\right)\right)^{1/3}} \ . \tag{22}$$

This relationship can also be inverted to

$$\underline{\underline{C}}^{-1} = \underline{\underline{q}}^{-1}\left(\det\left(\underline{\underline{q}}\right)\right)^{1/3} \ . \tag{23}$$

Based on these transformations, the Volterra derivative of any functional F with respect to the unconstrained conformation tensor $\underline{\underline{q}}$ may be expressed in terms of the Volterra derivative with respect to the constrained conformation tensor $\underline{\underline{C}}$ as

$$\frac{\delta F}{\delta q_{\alpha\beta}} = \frac{\delta F}{\delta C_{\gamma\varepsilon}}\frac{\delta C_{\gamma\varepsilon}}{\delta q_{\alpha\beta}} = \frac{1}{\left(\det q\right)^{1/3}}\frac{\delta F}{\delta C_{\gamma\varepsilon}}\left(\delta_{\alpha\gamma}\delta_{\beta\varepsilon} - \frac{1}{3}C_{\gamma\varepsilon}C^{-1}_{\alpha\beta}\right) = \frac{\delta F}{\delta C_{\gamma\varepsilon}}\left(\delta_{\alpha\gamma}\delta_{\beta\varepsilon} - \frac{1}{3}C_{\gamma\varepsilon}C^{-1}_{\alpha\beta}\right) , \tag{24}$$

with the last equality obtained by exploiting the fact that at the end $\underline{\underline{q}}$ can be set equal to $\underline{\underline{C}}$ and therefore the determinant of $\underline{\underline{q}}$ can be taken as unity. Note the Einstein summation convention is followed over repeated indices.

The Poisson bracket developed for an unconstrained conformation tensor $\underline{\underline{q}}$ in Beris & Edwards (1994 pp. 217-218), along with the momentum density $\underline{u}$ and the mass density ρ as internal variables, can now be re-expressed using Eq. (24) to the corresponding Poisson and dissipative bracket structures for a constrained single conformation contravariant tensor, $\underline{\underline{C}}$. The key point is that the transformation from the unconstrained brackets to determinant constrained brackets proceeds by replacing all Volterra derivatives with respect to $\underline{\underline{C}}$ in the former through Eq. (24). This approach guarantees the final expressions satisfy the Jacobi identity. Subsequently, the constrained Poisson bracket becomes

$$
\begin{aligned}
\{F,H\} = &-\int\left[\frac{\delta F}{\delta u_\gamma}\nabla_\beta\left(\frac{\delta H}{\delta u_\beta}u_\gamma\right)-\frac{\delta H}{\delta u_\gamma}\nabla_\beta\left(\frac{\delta F}{\delta u_\beta}u_\gamma\right)\right]d^3r\\
&-\int\left[\frac{\delta F}{\delta \rho}\nabla_\beta\left(\frac{\delta H}{\delta u_\beta}\rho\right)-\frac{\delta H}{\delta \rho}\nabla_\beta\left(\frac{\delta F}{\delta u_\beta}\rho\right)\right]d^3r\\
&-\int\left[\frac{\delta F}{\delta C_{\alpha\beta}}\frac{\delta H}{\delta u_\gamma}\nabla_\gamma C_{\alpha\beta}-\frac{\delta H}{\delta C_{\alpha\beta}}\frac{\delta F}{\delta u_\gamma}\nabla_\gamma C_{\alpha\beta}\right]d^3r\\
&+\frac{1}{3}\int C_{\alpha\beta}\left[\frac{\delta H}{\delta C_{\alpha\beta}}C^{-1}_{\rho\eta}\left(\frac{\delta F}{\delta u_\gamma}\right)\nabla_\gamma C_{\rho\eta}-\frac{\delta F}{\delta C_{\alpha\beta}}C^{-1}_{\rho\eta}\left(\frac{\delta H}{\delta u_\gamma}\right)\nabla_\gamma C_{\rho\eta}\right]d^3r\\
&-\int C_{\alpha\gamma}\left[\frac{\delta H}{\delta C_{\alpha\beta}}\nabla_\gamma\left(\frac{\delta F}{\delta u_\beta}\right)-\frac{\delta F}{\delta C_{\alpha\beta}}\nabla_\gamma\left(\frac{\delta H}{\delta u_\beta}\right)\right]d^3r\\
&-\int C_{\beta\gamma}\left[\frac{\delta H}{\delta C_{\alpha\beta}}\nabla_\gamma\left(\frac{\delta F}{\delta u_\alpha}\right)-\frac{\delta F}{\delta C_{\alpha\beta}}\nabla_\gamma\left(\frac{\delta H}{\delta u_\alpha}\right)\right]d^3r\\
&+\frac{2}{3}\int C_{\alpha\beta}\left[\frac{\delta F}{\delta C_{\alpha\beta}}\nabla_\gamma\left(\frac{\delta H}{\delta u_\gamma}\right)-\frac{\delta H}{\delta C_{\alpha\beta}}\nabla_\gamma\left(\frac{\delta F}{\delta u_\gamma}\right)\right]d^3r
\end{aligned}
\qquad . \qquad (25)
$$

The effect of the volume constraint is to modify the unconstrained Poisson bracket by introducing terms proportional to 1/3 in Eq. (25). We note that the fourth term on the right-hand side in the same equation has been omitted in the expressions given by Edwards *et al.* (2003). A similar form for the Poisson bracket, albeit restricted to incompressible flows, has also been proposed for the development of the MMG model (Grmela *et al.* 2014).

Similarly, the kernel for a general dissipative bracket $[F,H]$ which has been developed as the lowest order (bilinear) expression in terms of the Volterra derivatives for the unconstrained conformation tensor $\underline{\underline{q}}$ in Beris and Edwards (1994 pp. 219) is expressed as

$$\begin{aligned}
[F,H]_{wec} = &-\int \Lambda_{\alpha\beta\gamma\varepsilon}\left(\frac{\delta F}{\delta C_{\alpha\beta}}\left(\frac{\delta H}{\delta C_{\gamma\varepsilon}}-\frac{1}{3}C_{\rho\eta}\frac{\delta H}{\delta C_{\rho\eta}}C^{-1}_{\gamma\varepsilon}\right)-\frac{1}{3}C_{\rho\eta}C^{-1}_{\alpha\beta}\frac{\delta F}{\delta C_{\rho\eta}}\left(\frac{\delta H}{\delta C_{\gamma\varepsilon}}-\frac{1}{3}C_{\tau\upsilon}\frac{\delta H}{\delta C_{\tau\upsilon}}C^{-1}_{\gamma\varepsilon}\right)\right) d^3r \\
&-\int Q_{\alpha\beta\gamma\varepsilon}\left(\nabla_\alpha\frac{\delta F}{\delta u_\beta}\right)\left(\nabla_\gamma\frac{\delta H}{\delta u_\varepsilon}\right) d^3r \\
&-\int L_{\alpha\beta\gamma\varepsilon}\left(\nabla_\alpha\frac{\delta F}{\delta u_\beta}\left(\frac{\delta H}{\delta C_{\gamma\varepsilon}}-\frac{1}{3}C_{\rho\eta}\frac{\delta H}{\delta q_{\rho\eta}}C^{-1}_{\gamma\varepsilon}\right)-\nabla_\alpha\frac{\delta H}{\delta u_\beta}\frac{\delta F}{\delta C_{\gamma\varepsilon}}-\frac{1}{3}C_{\alpha\beta}C^{-1}_{\gamma\varepsilon}\nabla_\alpha\frac{\delta H}{\delta u_\beta}\frac{\delta F}{\delta C_{\alpha\beta}}\right) d^3r
\end{aligned} \quad , \quad (26)$$

where by kernel, symbolized here with the subscript *wec*, we mean "without entropy correction", i.e. without terms involving derivatives with respect to entropy. Such terms only affect non-isothermal flows which are not considered here.

In Eq. (26) we need to further specify $L_{\alpha\beta\gamma\varepsilon}$ using the expression provided in Beris and Edwards (1994 pp. 226)

$$L_{\alpha\beta\gamma\varepsilon} = -\frac{\xi}{2}\left(C_{\alpha\gamma}\delta_{\beta\varepsilon}+C_{\alpha\varepsilon}\delta_{\beta\gamma}+C_{\beta\gamma}\delta_{\alpha\varepsilon}+C_{\beta\varepsilon}\delta_{\alpha\gamma}\right), \quad (27)$$

where ξ is the usual non-affine parameter. This form gives rise to the Gordon-Schowalter derivative. The resulting dynamical equation for the constrained conformation tensor $\underline{\underline{C}}$ is then given from the above Poisson and dissipation brackets following the general practices outlined by Beris and Edwards (1994). More specifically, in order to derive the spatial form of the evolution equations for the variables, one uses the expression

$$\frac{dF}{dt} = \{F,H\}+[F,H] = \int\left(\frac{\partial\rho}{\partial t}\frac{\partial F}{\partial\rho}+\frac{\partial C_{\alpha\beta}}{\partial t}\frac{\partial F}{\partial C_{\alpha\beta}}+\frac{\partial u_\alpha}{\partial t}\frac{\partial F}{\partial u_\alpha}\right) d^3r \ , \quad (28)$$

to match against the relevant terms appearing in the Poisson and dissipative brackets, requiring the two expressions to give identical results for arbitrary functionals F. This is the same starting point in the MMG model (Grmela *et al.* 2014) albeit a more specific expression for the dissipation bracket is developed through the dissipation potential (Grmela 1984). In particular, applying this for $\underline{\underline{C}}$ contributions leads to the evolution equation for the conformation tensor as

$$\frac{D^{(\xi)}C_{\alpha\beta}}{dt}=\frac{2}{3}\xi C_{\alpha\beta}D_{\gamma\gamma}-\frac{2}{3}C_{\alpha\beta}\nabla_\gamma v_\gamma-\frac{1}{3}C_{\alpha\beta}C^{-1}_{\rho\eta}v_\gamma\nabla_\gamma C_{\rho\eta}-\Lambda_{\alpha\beta\gamma\varepsilon}\left(\frac{\delta H}{\delta C_{\gamma\varepsilon}}-\frac{1}{3}C_{\rho\eta}\frac{\delta H}{\delta C_{\rho\eta}}C^{-1}_{\gamma\varepsilon}\right)$$
$$+\frac{1}{3}\Lambda_{\rho\eta\gamma\varepsilon}C^{-1}_{\rho\eta}\left(\frac{\delta H}{\delta C_{\gamma\varepsilon}}-\frac{1}{3}C_{\nu\mu}\frac{\delta H}{\delta C_{\nu\mu}}C^{-1}_{\gamma\varepsilon}\right)C_{\alpha\beta} \quad . \tag{29}$$

It is easy to show that $\frac{D^{(\xi)}(\det(\underline{\underline{C}}))}{dt}=C^{-1}_{\alpha\beta}\frac{D^{(\xi)}C_{\alpha\beta}}{dt}=0$, and therefore demonstrate that this evolution equation automatically guarantees the invariance of the determinant of $\underline{\underline{C}}$. For incompressible and homogeneous flows, the expression above can be further simplified to

$$\frac{D^{(\xi)}C_{\alpha\beta}}{dt}=-\Lambda_{\alpha\beta\gamma\varepsilon}\left(\frac{\delta H}{\delta C_{\gamma\varepsilon}}-\frac{1}{3}C_{\rho\eta}\frac{\delta H}{\delta C_{\rho\eta}}C^{-1}_{\gamma\varepsilon}\right)+\frac{1}{3}\Lambda_{\rho\eta\gamma\varepsilon}C^{-1}_{\rho\eta}\left(\frac{\delta H}{\delta C_{\gamma\varepsilon}}-\frac{1}{3}C_{\nu\mu}\frac{\delta H}{\delta C_{\nu\mu}}C^{-1}_{\gamma\varepsilon}\right)C_{\alpha\beta} \quad . \tag{30}$$

In addition, the corresponding stress expression is given by

$$\sigma_{\alpha\beta}=Q_{\alpha\beta\gamma\varepsilon}\nabla_\gamma v_\varepsilon+2(1-\xi)C_{\beta\gamma}\frac{\delta H}{\delta C_{\alpha\gamma}}-\frac{2}{3}(1-\xi)C_{\rho\varepsilon}\frac{\delta H}{\delta C_{\rho\varepsilon}}\delta_{\alpha\beta} \quad . \tag{31}$$

The effect of the volume constraint is to introduce some new terms in the model so that the constraint $\frac{D^{(\xi)}(\det(\underline{\underline{C}}))}{dt}=0$ is duly satisfied under all circumstances. The expressions derived so far in Eqs. (29)- (31) describe the time derivative of $\underline{\underline{C}}$ and stress tensor $\underline{\underline{\sigma}}$. However, to proceed further, it is necessary to specify the form of the free energy, H, the fourth order viscosity matrix $Q_{\alpha\beta\gamma\varepsilon}$ as well as the fourth order relaxation tensor $\Lambda_{\rho\eta\gamma\varepsilon}$. Whereas for H one can use the underlying physics, no particular guidance exists for choosing the latter two. The approach taken in this work is to make these selections such that we can consistently recover a general functional form comparable to the asymptotic solutions of the microscopic flow around isolated ellipsoidal droplets to second order in Capillary number, as shown in Section 2.3. The next section focuses on examining the impact of the approximation used for the free energy expression as well as the various formulae chosen to represent the fourth order tensors that allow us to achieve the aforementioned objective.

3.3. The free energy expression

From continuum mechanics, the general dependence of a scalar, the internal energy, in terms of a tensor $\underline{\underline{C}}$ can be expressed by the following volume integral

$$E=\int g(I_1,I_2)dV \quad . \tag{32}$$

In general, the internal energy density g depends on all the invariants of the conformation tensor $\underline{\underline{C}}$. However, here it is only given as a function of the first two invariants since the third is constrained to be always 1. Beyond that, it has to best express the relevant physics. For emulsions, the internal energy is the interfacial energy of the droplets, and therefore g is taken to be equal to $N_D \gamma S_D$ where N_D is the number density of the droplets, γ is the surface tension and S_D is the surface area of each droplet. If no breakage or coalescence is assumed, the number density of droplets, N_D, is considered constant. In turn, S_D is expressed as a product of the area of the equilibrium droplet ($4\pi R^2$) and a dimensionless area $h(I_1, I_2)$, to be specified later. Thus

$$g(I_1, I_2) = \phi \Gamma h(I_1, I_2), \tag{33}$$

where $\Gamma \equiv 3\gamma / R$ is the surface energy density, R is the radius of the spherical droplet at equilibrium and ϕ is the volume fraction of the dispersed emulsion droplets. In this expression, $h(I_1, I_2)$ accounts for changes in area due to droplet deformation and for consistency, at equilibrium $h(I_1, I_2) = 1$.

The expression for the entropy of mixing functional, S_m, is given by

$$S_m = \int s_m(\phi) d\underline{r}\ , \tag{34}$$

where $s(\phi)$ is the entropy density that is a function of the volume fraction. This leads to the final complete expression for the Hamiltonian in terms of the constrained variable, $\underline{\underline{C}}$, is given by

$$H = \int \left(\frac{\underline{\underline{u}}^2}{\rho} + g(I_1, I_2) + h_s(T) s_m(\phi) \right) d\underline{r}\,, \tag{35}$$

where $h_s(T)$ is a free energy contribution from the solvent. Note that for a homogeneous isothermal system in which the volume fraction and temperature are constant such as that being considered here, the particular form of $s_m(\phi)$ and $h_s(T)$ are neither of concern nor a necessary input in the discussion and analysis that follows, and can safely be ignored.

The Volterra derivative of the free energy in Eq. (35) that belongs in the same vector subspace as the partial derivatives of conformation tensor $\underline{\underline{C}}$ is defined by

$$\frac{\delta H}{\delta C_{\alpha\beta}} = \Pi_{\alpha\beta\gamma\varepsilon} \frac{\partial g}{\partial C_{\gamma\varepsilon}}, \tag{36}$$

where the projector operator $\Pi_{\alpha\beta\gamma\varepsilon}$ for a system subject to a constraint $\det(\underline{\underline{C}}) = 1$ is given by

$$\Pi_{\alpha\beta\gamma\varepsilon} = \delta_{\alpha\gamma}\delta_{\beta\varepsilon} - \left(\frac{C^{-1}_{\gamma\varepsilon}}{C^{-1}_{\gamma\varepsilon}C^{-1}_{\gamma\varepsilon}}\right)C^{-1}_{\alpha\beta} \ . \tag{37}$$

The derivation of this projector-operator is provided in Appendix A. The partial derivative of g corresponding to the definition in Eq. (33) is given by

$$\frac{\partial g}{\partial C_{\gamma\varepsilon}} = \phi\Gamma\left(\left(\partial h/\partial I_1\right)\left(\delta_{\gamma\varepsilon}\right) + \left(\partial h/\partial I_2\right)\left(I_1\delta_{\gamma\varepsilon} - C_{\gamma\varepsilon}\right)\right) \ . \tag{38}$$

Consequently, the Volterra derivative of the free energy in the determinant constrained subspace is given by

$$\frac{\delta H}{\delta C_{\gamma\varepsilon}} = \phi\Gamma\left(\left(\partial h/\partial I_1\right)\left(\delta_{\gamma\varepsilon} - \left(\frac{I_2}{I_2^2 - 2I_1}\right)C^{-1}_{\gamma\varepsilon}\right) + \left(\partial h/\partial I_2\right)\left(I_1\delta_{\gamma\varepsilon} - C_{\gamma\varepsilon} - \left(\frac{I_1 I_2 - 3}{I_2^2 - 2I_1}\right)C^{-1}_{\gamma\varepsilon}\right)\right) \ . \tag{39}$$

It is noteworthy that this expression does not involve the entropic contribution to the free energy i.e. only the partial derivative of the interfacial free energy appears. This is physically meaningful since the entropy function only depends on the volume fraction and not on the shape of the ellipsoidal particles.

To make further progress, a specific expression for the normalized shape function is needed. Ideally, this should represent the surface of a general (tri-axial) ellipsoid whose axes are represented by the eigenvalues/eigenvectors of the conformation tensor $\underline{\underline{C}}$. However, an exact expression is difficult to obtain for the general case. Therefore, we propose to use Knud Thomsen's approximation (Xu *et al.* 2009) of the surface area as

$$\frac{S_D}{4\pi R^2} = h = \left(\frac{\lambda_1^{\omega/2}\lambda_2^{\omega/2} + \lambda_2^{\omega/2}\lambda_3^{\omega/2} + \lambda_3^{\omega/2}\lambda_1^{\omega/2}}{3}\right)^{\frac{1}{\omega}} , \tag{40}$$

where R is the equilibrium droplet radius, the λ_i's are the eigenvalues of $\underline{\underline{C}}$ and $\lambda_i^{1/2}$ represents the dimensionless semi-axis lengths of the ellipsoidal droplet. The value of ω may be determined by examining the error in the calculation of the surface area as shown in Appendix B. A value of $\omega = 8/5$ makes the expression in Eq. (40) asymptotically exact for small deviations from sphericity but also results in accurate estimates, typically within 1% error, even for highly deformed ellipsoid shapes (see Appendix B). Subsequently, using Eq. (40) for h (see Appendix C), one arrives at

$$\partial h/\partial I_1 = \frac{3^{-\frac{1}{\omega}}\left(\lambda_1^{\omega/2}\lambda_2^{\omega/2} + \lambda_2^{\omega/2}\lambda_3^{\omega/2} + \lambda_3^{\omega/2}\lambda_1^{\omega/2}\right)^{\frac{1}{\omega}-1}}{2\left(\lambda_1^2\lambda_2 - \lambda_1\lambda_2^2 - \lambda_1^2\lambda_3 + \lambda_2^2\lambda_3 + \lambda_1\lambda_3^2 - \lambda_2\lambda_3^2\right)}\left(\left(\lambda_1\lambda_2\right)^{\frac{\omega}{2}-1}\left(\lambda_2 - \lambda_1\right) + \left(\lambda_2\lambda_3\right)^{\frac{\omega}{2}-1}\left(\lambda_3 - \lambda_2\right) + \left(\lambda_1\lambda_3\right)^{\frac{\omega}{2}-1}\left(\lambda_1 - \lambda_3\right)\right)$$

, (41)

and

$$\partial h/\partial I_2 = \frac{3^{-\frac{1}{\omega}}\left(\lambda_1^{\omega/2}\lambda_2^{\omega/2}+\lambda_2^{\omega/2}\lambda_3^{\omega/2}+\lambda_3^{\omega/2}\lambda_1^{\omega/2}\right)^{\frac{1}{\omega}-1}}{2\left(\lambda_1^2\lambda_2-\lambda_1\lambda_2^2-\lambda_1^2\lambda_3+\lambda_2^2\lambda_3+\lambda_1\lambda_3^2-\lambda_2\lambda_3^2\right)}\left((\lambda_1\lambda_2)^{\frac{\omega}{2}}(\lambda_1-\lambda_2)+(\lambda_2\lambda_3)^{\frac{\omega}{2}}(\lambda_2-\lambda_3)+(\lambda_1\lambda_3)^{\frac{\omega}{2}}(\lambda_3-\lambda_1)\right)$$

, (42)

completing the definition of Eq. (39).

3.4. The viscosity term and final form of stress tensor

Furthermore, following usual practices applicable to dilute suspensions, the viscosity matrix $Q_{\alpha\beta\gamma\varepsilon}$ is selected to be isotropic, but with a suspension-dependent viscosity, which for dilute suspensions can be considered linear to the droplet volume fraction (Taylor 1932), as

$$Q_{\alpha\beta\gamma\varepsilon} = \mu\left(1+\phi P(\lambda)\right)\left(\delta_{\alpha\gamma}\delta_{\beta\varepsilon}+\delta_{\beta\gamma}\delta_{\alpha\varepsilon}\right). \quad (43)$$

As we shall show in the evaluation of the asymptotic model predictions for small *Ca* in section 3.6---see Eq. (52) below, this form of the viscosity matrix is powerful enough to guarantee consistency with the asymptotic theory presented in Eq. (13). In this expression, μ is the solvent viscosity and $P(\lambda)$ is a dimensionless factor dependent on the viscosity ratio λ that ends up being fully determined from the above-mentioned comparison to the asymptotic analysis results---see Eq. (66) below. In consequence, following the standard practices of the bracket formalism (Beris & Edwards 1994) the full expression for the extra stress tensor can be extracted from the given choices for the Poisson and dissipation bracket as

$$\sigma_{\alpha\beta} = 2\mu\left(1+\phi P(\lambda)\right)D_{\alpha\beta}+2\phi\Gamma\left(1-\xi\right)\left\{\left(\partial h/\partial I_1\right)\left(C_{\alpha\beta}-\frac{I_1}{3}\delta_{\alpha\beta}\right)+\left(\partial h/\partial I_2\right)\left(I_1C_{\alpha\beta}-C_{\alpha\gamma}C_{\gamma\beta}-\frac{2}{3}I_2\delta_{\alpha\beta}\right)\right\}, \quad (44)$$

with $\partial h/\partial I_1$ and $\partial h/\partial I_2$ determined according to Eqs. (41) and (42) respectively. The dependence of $P(\lambda)$ on the viscosity ratio will be discussed and elucidated by examining the asymptotic solution of the resultant model.

3.5. The relaxation term and final evolution equation for $\underline{\underline{C}}$

The final step in completing the model is to specify the fourth order tensor, $\underline{\underline{\underline{\underline{\Lambda}}}}$, appearing in Eq. (30) . As this is where most of the uncertainty lies, we use as guidance the symmetry properties that $\underline{\underline{\underline{\underline{\Lambda}}}}$ has to obey (see Beris and Edwards 1994 pp. 267-268) as well as, for simplicity, considering a linear superposition of the first three possible lowest order terms in $\underline{\underline{C}}$ as

$$\Lambda_{\alpha\beta\gamma\varepsilon} = \frac{3}{4I_2\tau_C\phi\Gamma}\begin{pmatrix} a_1\left(2\delta_{\alpha\gamma}\delta_{\beta\varepsilon}+2\delta_{\alpha\varepsilon}\delta_{\beta\gamma}\right)+ \\ a_2\left(C_{\alpha\gamma}\delta_{\beta\varepsilon}+C_{\alpha\varepsilon}\delta_{\beta\gamma}+C_{\beta\gamma}\delta_{\alpha\varepsilon}+C_{\beta\varepsilon}\delta_{\alpha\gamma}\right)+ \\ a_3\left(2C_{\alpha\gamma}C_{\beta\varepsilon}+2C_{\alpha\varepsilon}C_{\beta\gamma}\right) \end{pmatrix}, \tag{45}$$

where a_1, a_2 and a_3 are three scalar constants to be determined. As we shall show later on, this form of the relaxation matrix is of relatively low complexity yet sufficiently powerful to allow us in certain limits to obtain the dissipation corresponding to other models as well as to match the asymptotic theory in Eq. (13). The pre-factor in Eq. (45) is selected so as to facilitate subsequent manipulations while the weights, a_i, are dimensionless and in general may depend on the viscosity ratio of the emulsion droplet and suspending medium, and act to modify the overall relaxation time. The characteristic time $\tau_C = \mu R/\gamma$ is chosen for consistency with asymptotic theories that will be compared later on.

Using Eq. (45) together with Eq. (39) for the Volterra derivative of the free energy, the evolution equation for the constrained tensor $C_{\alpha\beta}$ in Eq. (30) can now be explicitly written as

$$\frac{D^{(\xi)}}{dt}C_{\alpha\beta} = -\frac{1}{\tau_C}\left\{\begin{array}{l} \left(\partial h/\partial I_2\right)\left(\begin{array}{l} a_1\left(\dfrac{3I_1}{I_2}\delta_{\alpha\beta}-2C^{-1}_{\alpha\beta}+\left(\dfrac{2}{3}\left(I_2^2-2I_1\right)-I_1\right)C_{\alpha\beta}\right)+ \\ a_2\dfrac{2}{I_2}\left(\left(\dfrac{I_1}{2}+\dfrac{I_2^2}{3}\right)C_{\alpha\beta}-\dfrac{3}{2}C_{\alpha\gamma}C_{\gamma\beta}-I_2\delta_{\alpha\beta}\right)+a_3\left(C_{\alpha\beta}-\dfrac{3}{I_2}\delta_{\alpha\beta}\right) \end{array}\right) \\ +\left(\partial h/\partial I_1\right)\left(\begin{array}{l} a_1\left(\dfrac{3}{I_2}\delta_{\alpha\beta}-\dfrac{I_1}{I_2}C^{-1}_{\alpha\beta}+\left(\dfrac{I_1}{3I_2}\left(I_2^2-2I_1\right)-1\right)C_{\alpha\beta}\right)+ \\ a_2\left(\dfrac{I_1}{3}C_{\alpha\beta}-\dfrac{I_1}{I_2}\delta_{\alpha\beta}\right)+a_3\left(\dfrac{3}{I_2}C_{\alpha\gamma}C_{\gamma\beta}-\dfrac{I_1}{I_2}C_{\alpha\beta}\right) \end{array}\right) \end{array}\right\}, \tag{46}$$

where use of the Cayley-Hamilton theorem is made. Eqs. (35), (44) and (46) are collectively referred to as the TCEE model.

Interestingly, the MM and MMG models, summarized below in Table 2, notwithstanding the deficiencies of the interpretation of the conformation tensor in the latter, can both be recovered as particular cases from Eq. (46) but using $h = I_2$ (which is not directly recoverable from our expression for the surface area, Eq. (40), as this is not compatible to the proper physical interpretation of the internal conformation tensor) for the dimensionless area and using $a_1 = a_2 = 0$; $a_3 = f_1$ for the MM model, where f_1 is defined by Maffettone and Minale (1998), or $a_1 = a_3 = 0$; $a_2 = I_2/2$ for the MMG model.

Evolution equations	$\frac{D^{(\xi)}}{dt}\underline{\underline{C}} = -\frac{1}{\tau}\left(\underline{\underline{C}} - \frac{3}{II_{\underline{\underline{C}}}}\underline{\underline{\delta}}\right)$	MM
	$\frac{D^{(\xi)}}{dt}\underline{\underline{C}} = -\frac{1}{\tau}\left(\left(\frac{I_{\underline{\underline{C}}}}{2} + \frac{II_{\underline{\underline{C}}}^2}{3}\right)\underline{\underline{C}} - \frac{3}{2}\underline{\underline{C}}\,\underline{\underline{C}} - II_{\underline{\underline{C}}}\underline{\underline{\delta}}\right)$	MMG
	$\frac{D^{(\xi)}}{dt}C_{\alpha\beta} = -\frac{1}{\tau}\left\{\begin{array}{l}(\partial h/\partial I_2)\left(\begin{array}{l} a_1\left(\frac{3I_1}{I_2}\underline{\underline{\delta}} - 2\underline{\underline{C}}^{-1} + \left(\frac{2}{3}\left(I_2^2 - 2I_1\right) - I_1\right)\underline{\underline{C}}\right) + \\ a_2\frac{2}{I_2}\left(\left(\frac{I_1}{2} + \frac{I_2^2}{3}\right)\underline{\underline{C}} - \frac{3}{2}\underline{\underline{C}}\cdot\underline{\underline{C}} - I_2\underline{\underline{\delta}}\right) + a_3\left(\underline{\underline{C}} - \frac{3}{I_2}\underline{\underline{\delta}}\right)\end{array}\right) \\ +(\partial h/\partial I_1)\left(\begin{array}{l} a_1\left(\frac{3}{I_2}\underline{\underline{\delta}} - \frac{I_1}{I_2}\underline{\underline{C}}^{-1} + \left(\frac{I_1}{3I_2}\left(I_2^2 - 2I_1\right) - 1\right)\underline{\underline{C}}\right) + \\ a_2\left(\frac{I_1}{3}\underline{\underline{C}} - \frac{I_1}{I_2}\underline{\underline{\delta}}\right) + a_3\left(\frac{3}{I_2}\underline{\underline{C}}\cdot\underline{\underline{C}} - \frac{I_1}{I_2}\underline{\underline{C}}\right)\end{array}\right)\end{array}\right\}$	TCEE
Free energy or Hamiltonian	-	MM
	$\mathrm{H} = \int \frac{\underline{u}^2}{\rho} + \frac{1}{4}k_B\mathrm{T}\chi\left(tr(\underline{\underline{C}})^2 - tr(\underline{\underline{C}}\cdot\underline{\underline{C}})\right) - k_B\mathrm{T}\chi\ln\det(\underline{\underline{C}})\,d^3r$	MMG
	$H = \int \frac{\underline{u}^2}{\rho} + \phi\Gamma h\left(I_1, I_2\right) + k_BT\left(\frac{3\phi}{4\pi R_D^3}\ln\phi + \frac{3(1-\phi)}{4\pi R_s^3}\ln(1-\phi)\right)d\underline{r} \equiv \int \Phi d\underline{r}$	TCEE
Interfacial Stress tensor	-	MM
	$\underline{\underline{\sigma}} = 4\chi\Gamma\left(1-\xi\right)\left(I_{\underline{\underline{C}}}\underline{\underline{C}} - \underline{\underline{C}}\cdot\underline{\underline{C}} - \frac{2}{3}II_{\underline{\underline{C}}}\underline{\underline{\delta}}\right)$	MMG
	$\underline{\underline{\sigma}} = 2\phi\Gamma\left(1-\xi\right)\left\{\left(\partial h/\partial I_1\right)\left(\underline{\underline{C}} - \frac{I_1}{3}\underline{\underline{\delta}}\right) + \left(\partial h/\partial I_2\right)\left(I_1\underline{\underline{C}} - \underline{\underline{C}}\cdot\underline{\underline{C}} - \frac{2}{3}I_2\underline{\underline{\delta}}\right)\right\}$	TCEE

TABLE 2. Comparison of the equations of the MM, MMG and TCEE models all in dimensionless form. Note that the MM model is phenomenological and therefore does not have a related stress tensor but may be coupled to the stress tensor of Batchelor (1970) for direct rheological predictions in the particular case when $\lambda = 1$.

3.6. *Asymptotic behavior of conformation tensor model*

The results of a perturbation expansion are now presented to demonstrate the TCEE model equations are in fact consistent with the microscopic theory presented in Eq. (13). The derivation of the

perturbation expansion of the conformation tensor $C_{\alpha\beta}$ in the small parameter, the characteristic time $\tau_C = \mu R/\gamma$, leads to

$$C_{\alpha\beta} = C_{0,\alpha\beta} + \tau_C C_{1,\alpha\beta} + \frac{\tau_C^2}{2} C_{2,\alpha\beta} + O(\tau^3) \ , \tag{47}$$

where

$$C_{\alpha\beta} = \delta_{\alpha\beta} \ , \tag{48}$$

$$C_{1,\alpha\beta} = \frac{2(1-\xi) D_{\alpha\beta}}{(a_1 + a_2 + a_3)(A_1 + A_2)} \ , \tag{49}$$

with

$$A_1 \equiv \partial h/\partial I_1\big|_{\tau_C=0} = \frac{\omega}{48}(2-\omega) \quad \text{and} \quad A_2 \equiv \partial h/\partial I_2\big|_{\tau_C=0} = \frac{\omega}{48}(2+\omega) \ , \tag{50}$$

and

$$C_{2,\alpha\beta} = \frac{2(1-\xi)}{(a_1 + a_2 + a_3)^2 (A_1 + A_2)^2} \left(\begin{array}{l} -2\left(\dfrac{DD_{\alpha\beta}}{dt} - \left(\Omega_{\alpha\gamma} D_{\gamma\beta} - D_{\alpha\gamma} \Omega_{\gamma\beta} \right) \right) + \\ \dfrac{2(1-\xi)}{(a_1 + a_2 + a_3)(A_1 + A_2)} \left(\begin{array}{l} \left(A_2 (6a_1 + 4a_2 + 2a_3) + A_1 (4a_1 + 2a_2) \right) D_{\alpha\gamma} D_{\gamma\beta} - \\ \dfrac{tr\left(\underline{\underline{DD}}\right)}{3} \left(A_2 (5a_1 + 3a_2 + a_3) + A_1 (3a_1 + a_2 - a_3) \right) \delta_{\alpha\beta} \end{array} \right) \end{array} \right) \tag{51}$$

.

Subsequently, substituting this result into the stress tensor in Eq. (44) results in

$$\underline{\underline{\sigma}} = 2\mu \underline{\underline{D}} + \phi\mu P(\lambda) 2\underline{\underline{D}} + \left(\frac{2\phi\Gamma \tau_C (1-\xi)^2}{(a_1 + a_2 + a_3)} \right) \left(2\underline{\underline{D}} - \frac{\tau_C}{(a_1 + a_2 + a_3)(A_1 + A_2)} \left\{ \begin{array}{l} 2\left(\dfrac{D}{Dt} \underline{\underline{D}} - \left(\underline{\underline{\Omega}} \cdot \underline{\underline{D}} - \underline{\underline{D}} \cdot \underline{\underline{\Omega}} \right) \right) \\ - \dfrac{4(1-\xi)(2a_1 + a_2)}{(a_1 + a_2 + a_3)} \left(\underline{\underline{D}} \cdot \underline{\underline{D}} - \dfrac{tr\left(\underline{\underline{D}} \cdot \underline{\underline{D}}\right)}{3} \underline{\underline{I}} \right) \end{array} \right\} \right)$$

$$+ O(\tau_C^3)$$

. (52)

For comparison to Eq. (52), Eq. (13) is rewritten in an analogous form given by

$$\underline{\underline{\sigma}} = 2\mu \underline{\underline{D}} + \phi \left(\frac{5\lambda + 2}{2(\lambda + 1)} \right) \mu \left(2\underline{\underline{D}} - \psi_1 \left\{ 2\left(\frac{D}{Dt} \underline{\underline{D}} - \left(\underline{\underline{\Omega}} \cdot \underline{\underline{D}} - \underline{\underline{D}} \cdot \underline{\underline{\Omega}} \right) \right) - \psi_2 \left(\underline{\underline{D}} \cdot \underline{\underline{D}} - \frac{tr\left(\underline{\underline{D}} \cdot \underline{\underline{D}}\right)}{3} \underline{\underline{I}} \right) \right\} \right) + O(Ca^2) , \tag{53}$$

where we also include a purely viscous term to account for the dissipation due to a solvent of viscosity μ. In this expression, the second order coefficients are (Schowalter, Chaffey & Brenner 1968)

$$\psi_1 = \left[\frac{Ca^*}{40} \left(\frac{(19\lambda+16)^2}{(\lambda+1)(5\lambda+2)} \right) \right], \tag{54}$$

and

$$\psi_2 = \frac{12(25\lambda^2+41\lambda+4)}{7(19\lambda+16)(\lambda+1)}, \tag{55}$$

where $Ca^* = \mu R / \gamma = \tau_C$.

It is important to realize that by comparing Eq. (52) and (53), they have the same form and all process dependent terms are common. This shows the consistency of the Non-Equilibrium Thermodynamics approach. In fact, full consistency can be achieved if the following constraint equations are satisfied:

$$\frac{2\Gamma\tau_C^2(1-\xi)^2}{(a_1+a_2+a_3)^2(A_1+A_2)} = \psi_1 \left(\frac{5\lambda+2}{2(\lambda+1)} \right) \mu, \tag{56}$$

$$\frac{4(1-\xi)(2a_1+a_2)}{(a_1+a_2+a_3)} = \psi_2, \tag{57}$$

and

$$\mu P(\lambda) + \frac{2\Gamma\tau_C(1-\xi)^2}{(a_1+a_2+a_3)} = \left(\frac{5\lambda+2}{2(\lambda+1)} \right) \mu. \tag{58}$$

In the section that follows, we use these expressions and other additional information, all available a-priori, to fully define all parameters of the TCEE model, at least in the limit of slow, slowly varying flows.

3.7. Determining model parameters from asymptotic solutions

In total, the model has 5 macroscopic parameters: ξ, $P(\lambda)$, a_1, a_2 and a_3. In general, there are many combinations of these parameters that may be used to develop a model that is consistent with the $O(Ca^2)$ expansion characterized by Eqs. (56)-(58), albeit involving some parameters as degrees of freedom that can be expanded even further if more involved expressions are used for the dissipation. Additional microscopic information on the morphology of the ellipsoid droplet, beyond agreement with the stress tensor to $O(Ca^2)$, is required to remove any ambiguity. To enforce such agreement with microscopic theory (Frankel & Acrivos 1970; Barthès-Biesel & Acrivos 1973; Rallison 1980) we first write the dimensionless form of Eq. (16) as

$$r^2 C_{ij}^{-1} n_i n_j = 1 , \tag{59}$$

where $n_i \equiv r_i / r$ and $r \equiv \left(r_i r_i \right)^{1/2}$ is the distance from the center of the ellipse to a position on its surface characterized by $\underline{r}$ such that $\left(n_i n_i \right)^{1/2} \equiv 1$. We note that r^2 and C_{ij} carry related information, but at different levels of description; the former is primarily used in microscopic theory while the latter is employed in macroscopic conformation tensor based models. Therefore, this relationship is important in enforcing consistency between microscopic and macroscopic descriptions of ellipsoidal morphology. It also allows us to determine additional constraints on the parameters in the model. By comparing the evolution of the first order perturbation to an equilibrium droplet, i.e. the evolution of $C_{1,\alpha\beta}$ in Eq. (47), to corresponding microscopic analysis of droplet deformation by Barthès-Biesel & Acrivos (1973) to $O(1)$ (Rallison 1981), we find that (see Appendix D)

$$\left(1 - \xi \right) = \frac{5}{\left(2\lambda + 3 \right)} \equiv f_1 , \tag{60}$$

and

$$\left(a_1 + a_2 + a_3 \right)\left(A_1 + A_2 \right) = \frac{40\left(\lambda + 1 \right)}{\left(19\lambda + 16 \right)\left(2\lambda + 3 \right)} \equiv f_2 . \tag{61}$$

These definitions ensure that the conformation tensor model is at least consistent with the $O(1)$ Taylor deformation theory at infinitesimal Capillary numbers. An immediate consequence of Eqs. (60) and (61) is that, asymptotically, the selection of $\omega = 8/5$ results in Eq. (56) being identically satisfied. This is very important as it provides an independent validation of the self-consistency of the proposed approach and a justification for the use of the more correct value of $\omega = 8/5$ in Eq. (40) for small deviations from sphericity (see Appendix B). Thus, we are left with only 4 independent equations (Eqs. (57), (58), (60) and (61)) to determine the model parameters.

To avoid the need for any adjustment right now we decide to use the lower order weight $a_1 = 0$. This allows us to develop a relaxation model with terms reminiscent of the MM and MMG models. The remaining 4 model parameters, ξ, $P(\lambda)$, a_2 and a_3, can then be fully determined from Eqs. (57), (58), (60) and (61) as

$$a_1 = 0 , \tag{62}$$

$$a_2 = \frac{\psi_2 f_2}{4 f_1 \left(A_1 + A_2\right)} \ , \tag{63}$$

$$a_3 = \frac{f_2}{\left(A_1 + A_2\right)} - \frac{\psi_2 f_2}{4 f_1 \left(A_1 + A_2\right)} \ , \tag{64}$$

$$\xi = 1 - \frac{5}{\left(2\lambda + 3\right)} \ , \tag{65}$$

and

$$P(\lambda) = \frac{\left(5\lambda + 2\right)}{2\left(\lambda + 1\right)} \left(1 - \frac{\left(19\lambda + 16\right)}{\left(5\lambda + 2\right)\left(2\lambda + 3\right)} \right) . \tag{66}$$

Note that all parameters depend on the viscosity ratio λ reflecting their dissipative nature. In the following, we present the results of the asymptotic model developed here and compare them against experimental data.

4. Application of the TCEE model to small Ca flows

In this section, the predictions of the TCEE model employing the parameters described in Section 3.7, as given by Eqs. (41), (42), (44), (46) and (62)-(66), are presented for a class of simple flows with prescribed kinematics for which other numerical and/or experimental results are available at small but finite *Ca* numbers to further evaluate the model.

4.1 Steady shear flows

In Figs. 2 and 3 we compare the TCEE model predictions for the principal stress components against numerical results from Kennedy *et al.* (1994) and the corresponding theoretical predictions of Showalter *et al.* (1968) in Eq. (13) for small *Ca* steady simple shear flows, for $\lambda = 1$ and $\lambda = 6.4$ respectively. Also presented for $\lambda = 1$ in Fig. 2, are results obtained from the droplet conformation predictions of the MM model through the use of stress expression obtained by Batchelor (1970) as given by Eq. 1.6 in Doi & Ohta (1991). Similar stress predictions for $\lambda = 6.4$ using this approach require information on the interface velocity and cannot be obtained without resorting to microscopic calculations. Therefore, the key advantage of the TCEE model (and thermodynamically consistent models in general) over phenomenological, solely structural, models like the MM model is that an accurate expression for the stress tensor can always be obtained directly through expressions like Eq. (44).

However, it is of interest to note that as seen in Fig. 2 for $\lambda = 1$ the predictions from the TCEE and MM models come to be very close, almost indistinguishable, especially at lower Ca. In retrospect, this is what one should have expected as both models are built up based on fitting asymptotic results, the MM model just for the conformation (because this is what is only involved there) and the TCEE model both for the conformation and stress. The fact that Batchelor's expression for stress comes so close to the TCEE model stress predictions provides additional evidence of the internal consistency of our approach which is fundamentally based on a connection between the stress and structure. The only difference being that in order to fully enforce this connection in our approach is that one requires independent results for the stress to fit the scalar parameters involved in the model. In exchange, what one gets with this approach of indirectly enforcing the connection between the stress and structure as opposed to using a direct relationship as that of Batchelor (1970) is an easier evaluation and a more general one valid for all λ values, instead of just $\lambda = 1$. In both Figs. 2 and 3, the TCEE model captures well the trends in the numerical results especially at the small Ca numbers for which the model parameters have been developed. Furthermore, the predictions of the rheology at larger Capillary number are reasonable and demonstrate the robustness of the TCEE model.

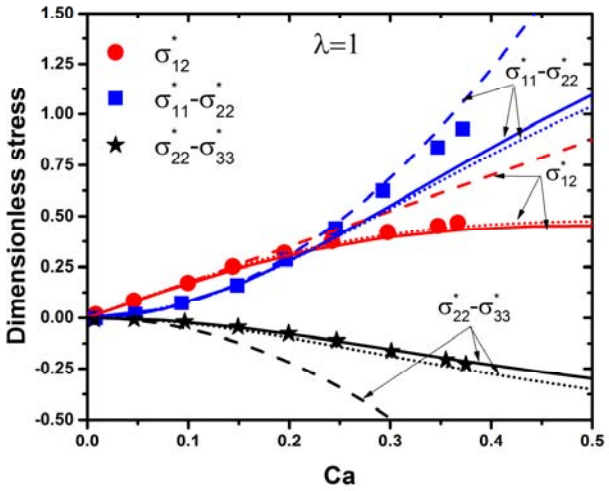

FIGURE 2. Model predictions of the stress tensor components as a function of Capillary number (Ca) compared against simulation results (symbols) from Kennedy et al. (1994) for $\lambda = 1$. Solid lines are TCEE model predictions using Eq. (44), dotted lines are predictions from MM model using the stress expression of Batchelor (1971) and dashed lines are predictions from asymptotic theory in Eq. (13). In applying Eqs. (13) and (44), the dissipation of the medium is neglected and the stress tensor is scaled by the interfacial energy density γ / R such that $\sigma^*_{\alpha\beta} = \sigma_{\alpha\beta} \mathrm{R}/\gamma$.

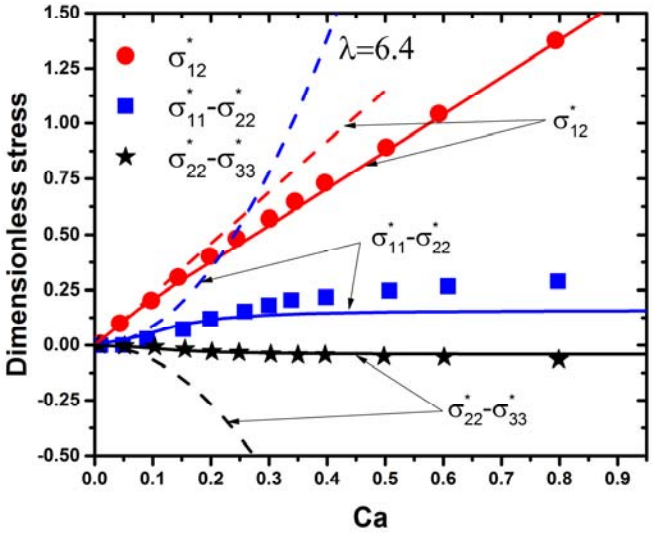

FIGURE 3. Model predictions of the stress tensor components as a function of Capillary number (Ca) compared against simulation results (symbols) from Kennedy et al. (1994) for $\lambda = 6.4$. Solid lines are TCEE model predictions using Eq. (44) while dashed lines are predictions from asymptotic theory in Eq. (13). In applying Eqs. (13) and (44), the dissipation of the medium is neglected and the stress tensor is scaled by the interfacial energy density γ / R such that $\sigma^*_{\alpha\beta} = \sigma_{\alpha\beta}\,\mathrm{R}/\gamma$.

In Figs. 4a and 4b, we present the TCEE model predictions of the Taylor deformation parameter defined as

$$D_T = \frac{(L-B)}{(L+B)}\,, \tag{67}$$

where L and B are the semi-axes of the emulsion droplet projected in the flow-gradient plane, for $\lambda = 1$ and $\lambda = 6.4$, respectively. Note that as far as the TCEE model is concerned, its predictions for steady simple shear flow involve a structure with mirror symmetry with respect to the flow-gradient plane. Thus in this case L and B are the major and minor axis of the ellipsoid as shown in Fig. 1. In Figs. 4c and 4d, we present the TCEE model predictions for the droplet orientation angle θ relative to the flow direction for the same values of λ. Also included in the same figure for comparison purposes are simulation results of Kennedy *et al.* (1994), the MM model predictions and theoretical calculations, to first order, of the Taylor deformation parameter given as (Taylor 1934)

$$D_T = \frac{19\lambda + 16}{16\lambda + 16} Ca\,, \tag{68}$$

and of the orientation angle in simple shear flow given as (Chaffey & Brenner 1967)

$$\theta = \frac{\pi}{4} - \frac{(2\lambda+3)(19\lambda+16)}{80(\lambda+1)} Ca \ . \tag{69}$$

The TCEE model and MM model provide similar predictions of the trends observed in the experimental data at small Capillary numbers. However, at larger Capillary numbers, the non-linear effects entering the two models are distinct, and the predictions from the two models are slightly different. This is not surprising because although the relaxation terms in the two models differ, the parameters entering the conformation tensor equation in both models are selected to be consistent with the results of Barthès-Biesel & Acrivos (1973) to O(1) in Ca number only. Therefore, the distinct advantage of the TCEE model is that in addition to providing equally good approximations of the droplet deformation and orientation as in the previous MM model, it also provides good predictions of the stress tensor at all viscosity ratios as shown in Figs. 2 and 3.

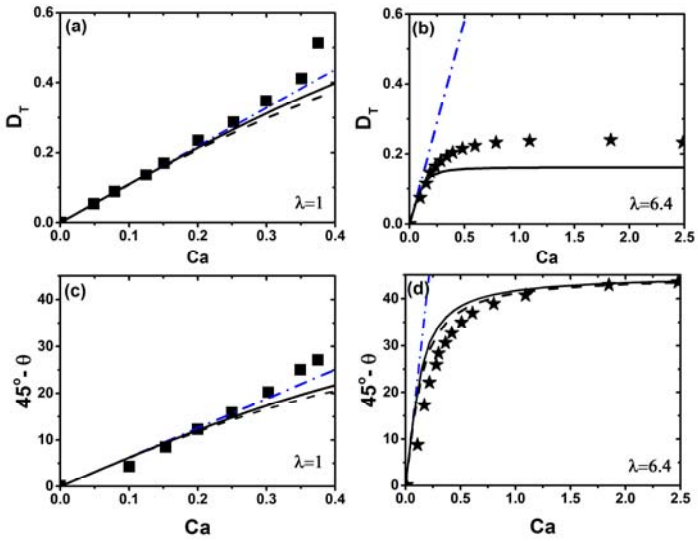

FIGURE 4. Model predictions of the droplet deformation D_T (Figs. (a) and (b)) and orientation angle θ (Figs. (c) and (d)) as a function of Capillary number (Ca) compared against simulation results (symbols) from Kennedy et al. (1994) for $\lambda = 1$ (Figs. (a) and (c)) and $\lambda = 6.4$ (Figs. (b) and (d)). Also shown with dot-dashed lines in Figs. (a) and (b) are theoretical results by Taylor (1934) for the deformation parameter using Eq. (68) and in Figs. (c) and (d) theoretical results by Chaffey & Brenner (1967) using Eq. (69) for the orientation angle. Solid lines are TCEE model predictions and dashed lines are MM model predictions.

As seen, in Figs. 4a and 4c, for $\lambda = 1$ the TCEE model predictions of the droplet deformation and orientation are in good agreement with the experimental data. However, as seen in Figs. 4b and 4d, for $\lambda = 6.4$ the TCEE model shows larger deviations from the experimental data albeit, in this case, the agreement is much better than that of the asymptotic results that clearly miss the observed trends. The

much better agreement seen in the corresponding stress predictions from the TCEE model in Fig. 3 for $\lambda = 6.4$ may be partly attributed to the fact that the TCEE model stress predictions are forced to be consistent with the stress tensor results of Showalter et al. (1968) to $O(Ca^2)$. On the other hand, the conformation tensor results are only enforced to be $O(1)$ accurate with respect to the results of Barthès-Biesel & Acrivos (1973). This may partly explain the relatively weaker agreement seen in Figs. 4b and 4d for $\lambda = 6.4$ between the TCEE model and simulation results for the droplet deformation and orientation as compared to that seen in Figs. 4a and 4b for $\lambda = 1$. More specifically, as the viscosity ratio increases, non-linear effects on the droplet deformation (that require a complex description of the non-affine motion) may be more important. Still the improvement over the asymptotic results from which the TCEE model emerges is impressive.

As previously noted, the agreement between the TCEE model and the simulation data may be improved by introducing additional corrective terms. For example, such corrective effects may be introduced into the model through more complex dissipative terms in the TCEE model that are selected to be consistent with the results of Barthès-Biesel & Acrivos (1973) to higher order. On the other hand, although better predictions for simple shear flow can also be achieved by allowing for a non-linear dependence of ξ on the Capillary number, this is a change that destroys the thermodynamic consistency of the model. This can result in aphysical predictions in more general flows. Ultimately, this brings out the important point that the conformation tensor equation and the expression for stress tensor are not independent in the context of a thermodynamically consistent model. Therefore, care must be exercised when modifying model parameters. As a result, we do not attempt any phenomenological modification to ξ based on the Capillary number. Modifications based on the conformation tensor through the invariants as well as additional non-linearity in the dissipation are allowed, but we delegate such improvements to a future publication in order to keep the analysis here as simple as possible. On the other hand, for $\lambda = 1$ non-affine effects are less important and the $O(1)$ approximation of the results of Barthès-Biesel & Acrivos (1973) used to develop some of the TCEE model parameters is more accurate. Consequently, the TCEE model predictions for the droplet deformation, orientation and stress tensor in Figs. 4a, 4c and 2, respectively, provide a good representation of the numerical results in this case.

Next, the TCEE model predictions are compared against experimental data for the droplet deformation and orientation from Torza *et al.* (1972) in a dilute emulsion of oxidized Castor oil in two different Silicone oils corresponding to $\lambda = 0.08$ and $\lambda = 3.6$. In Fig. 5 we compare the TCEE model predictions for droplet deformation and orientation against the experimental data as well as the predictions of the MM model. Note again that both the TCEE and MM models provide similar predictions

of the trends observed in the experimental data for similar reasons discussed before relation to the predictions shown in Fig. 4. Moreover, in Fig. 5, similar to the comparison against the numerical results Kennedy *et al.* (1994) in Fig. 4, the comparison of the model predictions of the Taylor deformation parameter against the experimental data of Torza *et al.* (1972) for high viscosity ratios becomes poor as the Capillary number increases. Similar to the comments appearing in the previous paragraph, the agreement can be improved by using the non-linear extension of ξ by allowing a direct dependence on the Capillary number as in the MM model (Maffettone & Minale 1998). However, as mentioned before, this comes at the risk of aphysical behavior in more general flows. An additional remark that can be made based on both Figs. 4 and 5, is that the TCEE model predictions (and those of the original MM model) work best for $\lambda \leq 1$. The less satisfactory agreement with experimental and numerical data at higher viscosity ratios may be attributed to the increasing importance of non-affine effects as the droplets effectively become more rigid. As a concluding remark, there is a clear need to work on better non-affine representations but only if they are compatible with the bracket scheme followed in this work in order to avoid aphysical results.

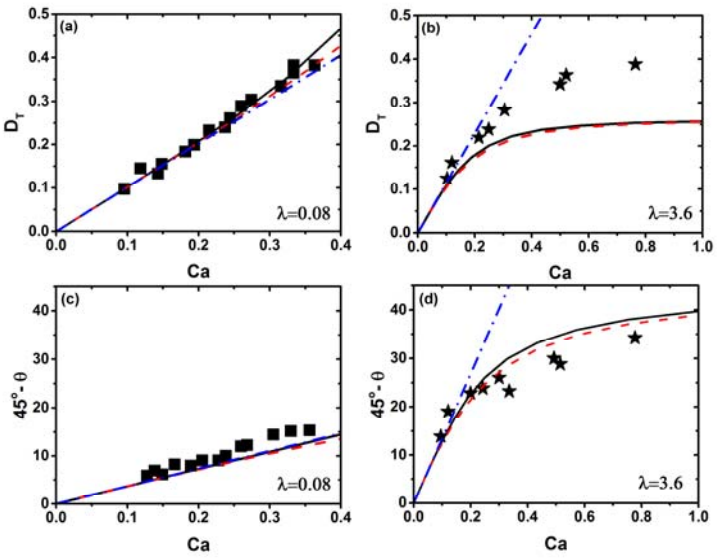

FIGURE 5. Model predictions of the droplet deformation D_T (Figs. (a) and (b)) and orientation angle θ (Figs. (c) and (d)) as a function of Capillary number (Ca) compared against experimental results (symbols) from Torza et al. (1972) for $\lambda = 0.08$ (Figs. (a) and (c)) and $\lambda = 3.6$ (Figs. (b) and (d)). Also shown with dot-dashed lines in Figs. (a) and (b) are theoretical results by Taylor (1934) for the deformation parameter using Eq. (68) and in Figs. (c) and (d) theoretical results by Chaffey & Brenner (1967) using Eq. (69) for the orientation angle. Solid lines are TCEE model predictions and dashed lines are MM model predictions.

Finally, for completion, in Table 2 the numerical values of the parameters corresponding to the predictions of the TCEE model in Fig. 5 are summarized. The presence of a negative value for a_3 may raise concerns regarding the thermodynamic admissibility of this parameter value. This is examined by investigating whether the thermodynamic consistency criterion requiring a positive relaxation dissipation density, given by

$$\Phi = \Lambda_{\alpha\beta\gamma\varepsilon}\left(\frac{\delta H}{\delta C_{\gamma\varepsilon}} - \frac{1}{3}C_{\rho\eta}\frac{\delta H}{\delta C_{\rho\eta}}C^{-1}_{\gamma\varepsilon}\right)\left(\frac{\delta H}{\delta C_{\alpha\beta}} - \frac{1}{3}C_{\rho\eta}\frac{\delta H}{\delta C_{\rho\eta}}C^{-1}_{\alpha\beta}\right) \geq 0 \ , \tag{70}$$

is satisfied in this case. This measure has been computed numerically, as a function of the Capillary number, and is found to be always positive. Moreover, a negative value of $P(\lambda)$ such as that seen in the first column of Table 2 is admissible as long as the overall effective viscosity remains positive which can certainly be enforced in the case of the dilute limit $\phi \to 0$, as the contribution of the $P(\lambda)$ term in the viscosity is weighted by ϕ (see Eq. (44)).

	$\lambda = 0.08$	$\lambda = 3.6$
a_2	0.62	1.71
a_3	5.21	-0.11
ξ	-0.58	0.51
$P(\lambda)$	-1.45	1.274

TABLE 2. Summary of model parameters corresponding to microstructure predictions of TCEE model in Fig. 5.

4.2 Transient simple shear flow

So far, the numerical and experimental data sets used to validate the TCEE model have been steady state shear flow results. In this subsection, the TCEE model is compared against time dependent shear flow experiments (Guido & Villone 1998) obtained using a dilute emulsion system of polyisobutylene (PIB) and polydimethylsiloxane (PDMS) with $\lambda = 1.4$. In Fig. 6 we examine the evolution of the three dimensionless droplet semi-axes as a function of strain in the startup of shear flow for $Ca = 0.24$ and $\lambda = 1.4$. Note that the TCEE model predictions agree very well with the experimental data and describing the principal axes of the deforming droplet better than the MM model. Experimental results such as those in Fig. 6 are important in distinguishing the predictive capability of the two models as it is well known that the Taylor deformation parameter D_T, defined in Eq. (67), is not a rigorous measure of the droplet

deformation. Therefore, unlike the experimental results for droplet deformation in Figs. 4 and 5 which are inconclusive, the comparison in Fig. 6 shows that the TCEE model provides significantly better predictions of the dimensionless semi-axes of the deforming droplet than the MM model.

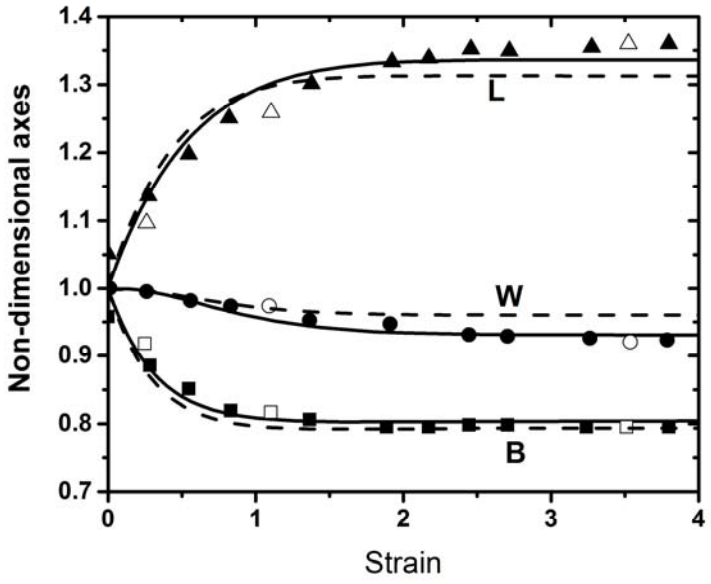

FIGURE 6. Model predictions for the three non-dimensional axes of the droplet as a function of applied strain for transient start-up shear flow corresponding to $Ca = 0.24$ and $\lambda = 1.4$ compared against experimental data. Open and filled symbols correspond to experiments at two different digitization settings (Guido & Villone 1998). Solid lines correspond to predictions of TCEE model and dashed lines correspond to predictions of MM model.

4.3 Steady state flow in a four-roll mill

Here we compare the TCEE model predictions for the deformation and orientation of a droplet against experimental results of Bentley and Leal (1986) obtained through the use of a four-roll mill device. In these experiments, the velocity gradient tensor around the droplet is steady and defined as

$$\underline{\underline{\nabla v}} = \frac{1}{2}\dot{\gamma}\begin{bmatrix} 1+\alpha & 1-\alpha & 0 \\ -1+\alpha & -1-\alpha & 0 \\ 0 & 0 & 0 \end{bmatrix}, \tag{71}$$

where the dimensionless parameter $0 \le \alpha \le 1$ specifies the relative strength of the strain rate and vorticity in the flow. The limit of $\alpha = 1$ represents purely straining flow while $\alpha = 0$ represents simple shear flow. In Fig. 7, we compare the TCEE model predictions against the experimental results of Bentley and Leal (1986) as well as against the predictions of the MM model for the deformation (Fig. 7a) and orientation (Fig. 7b) of a droplet in the flow field defined in Eq. (71). As shown there, the TCEE model captures well

the deformation observed at low Capillary numbers but its predictions deviate from experimental data as the Capillary number increases. The deviation of the model from the experimental data occurs when an upturn is observed in the experimentally measured deformation parameter prior to breakup. Under these circumstances, the actual droplet shape is expected to begin to deviate significantly from an ellipsoidal shape which violates a critical assumption of the TCEE model. Therefore, at larger Ca, the TCEE model is not expected to describe the real system. Still, the success of the model at small Capillary numbers indicates the utility of employing asymptotic theory in constraining the small Capillary number response of the TCEE model. Note that for those small Ca values the predictions of the TCEE and MM models are practically indistinguishable.

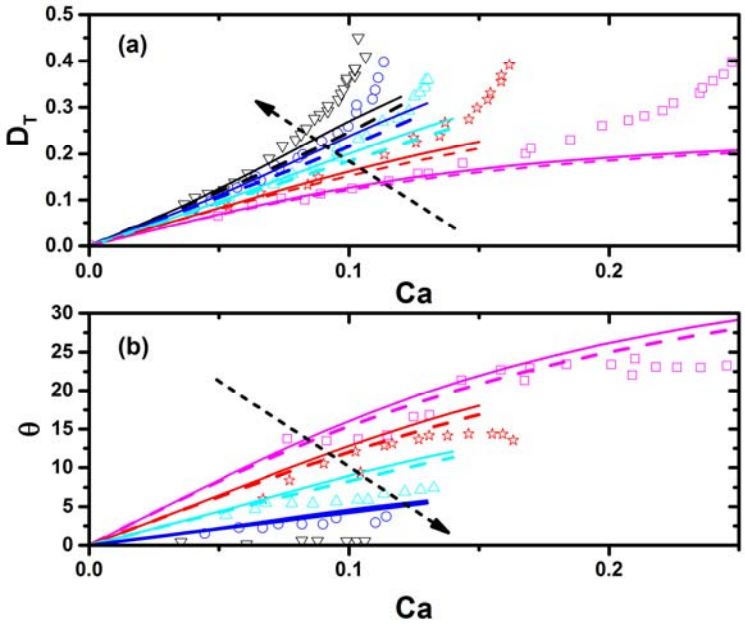

FIGURE 7. Model predictions of (a) the droplet deformation, D_T, and (b) orientation angle, θ, as a function of Ca for $\lambda = 6.5$ compared against experimental data. Experimental data (symbols) from Bentley and Leal (1986). Arrows indicate an increasing value of the flow parameter α defined by Eq. (71) assuming the values 0.2, 0.4, 0.6, 0.8 and 1. Solid lines correspond to predictions of TCEE model and dashed lines correspond to predictions of MM model.

5. Conclusions

In this work, we developed an internal conformation tensor-based macroscopic rheological model for dilute emulsions through a rigorous and systematic bracket theory. We started by first probing the consequences of the microscopic physical interpretation of the conformation tensor that was chosen to describe approximately the deformed droplet geometry as an ellipsoid. This microscopic interpretation was first used to independently construct an extended free energy expression for a dilute emulsion. This

expression takes into account the surface free energy of the deformed droplets and can conveniently be evaluated in a closed form based on a powerful approximation for the surface of an ellipsoid in terms of the first and second invariants of the conformation tensor. Following the definition of the conformation tensor for infinitesimal deformations under conditions for which there is purely affine motion, we then demonstrated its contravariant tensorial character since, under those conditions, it coincides with the (contravariant) Cauchy-strain tensor. The appropriate Poisson bracket was then developed by suitably modifying the standard Poisson bracket for contravariant tensors taking into account the unit determinant constraint imposed due to the droplet volume conservation. That constraint modifies the dissipation bracket as well, from which a general low order (in Volterra derivatives with respect to the conformation tensor) expression that was developed in terms of a minimum of four dissipation parameters. The final model that resulted as a consequence to the application of the Poisson and dissipation bracket dynamics, was then shown to be capable of providing asymptotic predictions for the flow induced structures and extra stress that are fully consistent with available asymptotic theories for both the internal droplet structure and the macroscopic extra stress tensor. We took advantage of this result to use these asymptotic theories to fully determine all four dissipation model parameters. Then we validated the model through comparisons against experimental and simulation data for small Capillary number in various flows with pre-specified kinematics ranging from steady and transient simple shear to a linear combination of simple shear and pure straining flow. In all cases, the TCEE model produces results that are physical and reliably extend the asymptotic results valid at infinitesimally small Capillary number to small but finite values.

Comparisons of the TCEE model evolution equation against the MM model of Maffettone & Minale (1998) and the MMG model of Grmela *et al.* (2014) reveals these as particular subcases corresponding to particular approximations for the free energy and particular selections of the relaxation dissipation. Still we need to note here that the similarity is only apparent as the expressions that need to be used for the free energy in the MM and MMG models in order to conform to our general form of the dissipation are in this case artificial and not compatible with the underlying physics. Moreover, we should also note that the proposed free energy expression in the MMG model is based on a very different microscopic interpretation for the conformation tensor that requires it in this case to be the square root of the one used in the TCEE and MM models. In this way, we can say that the TCEE model provides not only a systematic generalization of these two previous contravariant tensor approaches but a completion (in terms of the MM model) and a correction (regarding the MMG model). Moreover, the model parameter selection for the TCEE model proposed in this work makes it the only approach that is

consistent with available asymptotic theories for both the conformation and stress tensor in the limit of small Capillary number shear flows. We also note that if the same procedure used to determine the model parameters in the TCEE model is repeated using the macroscopic MMG model equations (Grmela *et al.* 2014) one can only match the asymptotic result of Schowalter *et al.* (1968) to $O(Ca)$. Therefore, the form of the TCEE model discussed in the preceding sections is more general and more consistent with microscopic theory, a clear advantage over the MMG model.

Reasonable agreement between model predictions and experimental/numerical data is also demonstrated for finite Capillary number shear flows. Furthermore, the TCEE model is also applicable to arbitrary flows, underlying the usefulness of the conformation tensor approach. To extend the model application to larger Ca numbers, additional non-linear effects may be incorporated by using higher order expressions for $L_{\alpha\beta\gamma\varepsilon}$ and $\Lambda_{\alpha\beta\gamma\varepsilon}$ such that the limiting expressions are consistent with higher order microscopic theory results and/or finite Ca number data. Such modifications are outside the scope of this work and will be addressed in a future publication.

To the best of our knowledge, this is the first time that a conformation-based model proposed for dilute droplet suspensions has been rigorously developed from first principles and systematically validated through comparison against microscopic asymptotic results for stress and structure, allowing for the self-consistent evaluation of all model parameters and complete elimination of any adjustable parameters. In some ways, this is analogous to efforts to develop conformation-based theories for polymer solutions based on a microscopic dumbbell model. Therefore, the approach taken here shows the natural next step towards developing the next generation of macroscopic suspension models that go beyond the infinitesimal Ca limit, which is the only one that can be captured well through the use of an effective viscosity generalized Newtonian model. As we look to describe complex suspension behavior, it is clear that the use of a conformation tensor that is consistently tied to the underlying structure helps to explain its time evolution and better describe the rich rheological suspension behavior. Furthermore, the use of the bracket formalism helps to enforce thermodynamic admissibility and naturally connects the stress to the underlying structure thereby significantly extending the validity of previously independently developed microscopic asymptotic relations. We showed this for a particular case of a monodisperse dilute emulsion. A lot more work remains to be done, especially in parallel with efforts in computer based microscopic simulations and analytic asymptotic solutions under more general flows. Hopefully, such efforts can take advantage of the framework outlined here, to develop a more complete macroscopic level description of suspension behavior.

Acknowledgments

This material is based upon work supported by the National Science Foundation under Grant No. CBET 312146. Any opinions, findings, and conclusions or recommendations expressed in this material are those of the author(s) and do not necessarily reflect the views of the National Science Foundation.

Appendix A

This appendix describes the proper formulation of functional derivatives in a vector subspace subject to a constraint on the determinant of the conformation tensor. The enforcement of a unit determinant constraint imposes the restriction that all functional derivatives must also belong to the same operating subspace as the constrained variable $C_{\alpha\beta}$ (Beris & Edwards 1994). More specifically, the task is to define a projector operator $\Pi_{\alpha\beta\gamma\varepsilon}$ such that

$$\frac{\delta H}{\delta C_{\alpha\beta}} = \Pi_{\alpha\beta\gamma\varepsilon} \frac{\partial h}{\partial C_{\gamma\varepsilon}} \,, \tag{A 1}$$

where $H = \int h d\underline{r}$, H is a functional e.g. the Hamiltonian and h is the energy density which is a function of $C_{\alpha\beta}$. The development of the correct projector operator can be accomplished by analogy to examining the restriction of vectors to a subspace S as presented schematically in Fig. A1.

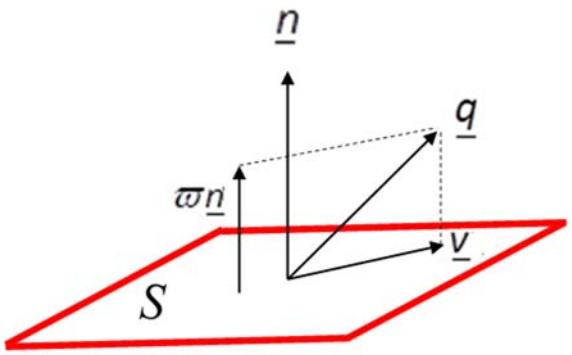

FIGURE A1. A schematic describing the decomposition of an arbitrary vector $\underline{q}$ into its normal, $\varpi\underline{n}$, and tangential, $\underline{v}$, components with respect to a given subspace S.

Let S be a subspace that contains vectors $\underline{v}$ such that for any non-zero vector $\underline{n}$, $\underline{n}\cdot\underline{v} = 0$. This can be expressed concisely as

$$S := \left\{ \underline{v} : \underline{n}\cdot\underline{v} = 0 \right\}. \tag{A 2}$$

Consequently, the expression for the projection $\underline{v}$ to the subspace S of any arbitrary vector $\underline{q}$ is

$$\underline{v} = \underline{\underline{\Pi}}\cdot\underline{q} = \underline{q} - \varpi\underline{n} = \underline{q} - \left(\frac{\underline{q}\cdot\underline{n}}{\underline{n}\cdot\underline{n}} \right)\underline{n}, \tag{A 3}$$

where $\underline{\underline{\Pi}} \equiv \underline{\underline{\delta}} - \frac{1}{(\underline{n}\cdot\underline{n})}\underline{n}\underline{n}$. The result in Eq. (A 3) can be used to define by analogy the projection $\frac{\delta H}{\delta C_{\alpha\beta}}$ of $\frac{\partial h}{\partial C_{\alpha\beta}}$ following Eq. (A 1) as follows. The identification of the normal characterizing the determinant constrained tensor subspace is made by considering the time derivative of $\det(\underline{\underline{C}}) = 1$:

$$\frac{d(\det(\underline{\underline{C}}))}{dt} = C^{-1}_{\alpha\beta}\frac{dC_{\alpha\beta}}{dt} = 0 \ . \tag{A 4}$$

If properly formulated, $\frac{dC_{\alpha\beta}}{dt}$ is the evolution equation for the constrained tensor $C_{\alpha\beta}$ implying it lives in the determinant constrained matrix subspace and $C^{-1}_{\alpha\beta}$ is the normal tensor that characterizes this subspace just as $\underline{n}$ is the normal vector that characterizes S. Therefore, the following identifications can be made:

$$C^{-1}_{\alpha\beta} \quad \leftrightarrow \quad \underline{n}; \qquad \frac{\partial h}{\partial C_{\alpha\beta}} \quad \leftrightarrow \quad \underline{q}; \qquad \frac{\delta H}{\delta C_{\alpha\beta}} \quad \leftrightarrow \quad \underline{v}; \ , \tag{A 5}$$

from which the projector operator becomes

$$\Pi_{\alpha\beta\gamma\varepsilon} = \delta_{\alpha\gamma}\delta_{\beta\varepsilon} - \left(\frac{C^{-1}_{\gamma\varepsilon}}{C^{-1}_{\gamma\varepsilon}C^{-1}_{\gamma\varepsilon}}\right)C^{-1}_{\alpha\beta} \ . \tag{A 6}$$

Appendix B

This appendix examines the predictions of Knud Thomsen's formula (Xu *et al.* 2009) for the surface area of an ellipsoid with semi-axes of lengths a, b and c, Eq. (40) with $R = \sqrt[3]{3V/(4\pi)} = \sqrt[3]{abc}$ and $\lambda_1 = (a/R)^2$, $\lambda_2 = (b/R)^2$ and $\lambda_3 = (c/R)^2$. First we make the comparisons against available analytical results for the particular case of a spheroid corresponding to $a = b$ (Beyer 1987):

$$\frac{S_D}{4\pi R^2} = \begin{cases} \frac{1}{2}\left(\frac{a}{c}\right)^{\frac{2}{3}}\left(1 + \frac{1-e^2}{e}\tanh^{-1}(e)\right) \ ; \ e^2 = \left(1 - \left(\frac{c}{a}\right)^2\right) \text{ for } a = b > c \text{ (oblate spheroid)} \\ \frac{1}{2}\left(\frac{a}{c}\right)^{\frac{2}{3}}\left(1 + \frac{c}{ae}\sin^{-1}(e)\right) \ ; \ e^2 = \left(1 - \left(\frac{a}{c}\right)^2\right) \text{ for } a = b < c \text{ (prolate spheroid)} \end{cases} \ . \tag{B 1}$$

For comparison purposes it is useful to define the sphericity parameter ε as

$$\varepsilon = \begin{cases} \left(\frac{a}{c}\right)^{\frac{1}{3}} - 1 & \text{for } a = b > c \text{ (oblate spheroid)} \\ \left(\frac{c}{a}\right)^{\frac{1}{3}} - 1 & \text{for } a = b < c \text{ (prolate spheroid)} \end{cases} \tag{B 2}$$

In Fig. B1, the value of ω that minimizes the error arising from Knud Thomsen's formula at fixed ε, $\omega_{optimum}$, is presented. For either the prolate or oblate spheroid, it is clear that as $\varepsilon \to 0$, $\omega_{optimum} \to 8/5$ at which case the Knud Thomsen formula becomes exact. This suggests that this is the appropriate choice for using in the asymptotic analysis of droplet deformation. However, note that for this value, the error remains small for up to $O(1)$ values of the sphericity parameter. For example, for the oblate case considered next, for $\varepsilon = 0.26$ the error is less than 0.1%.

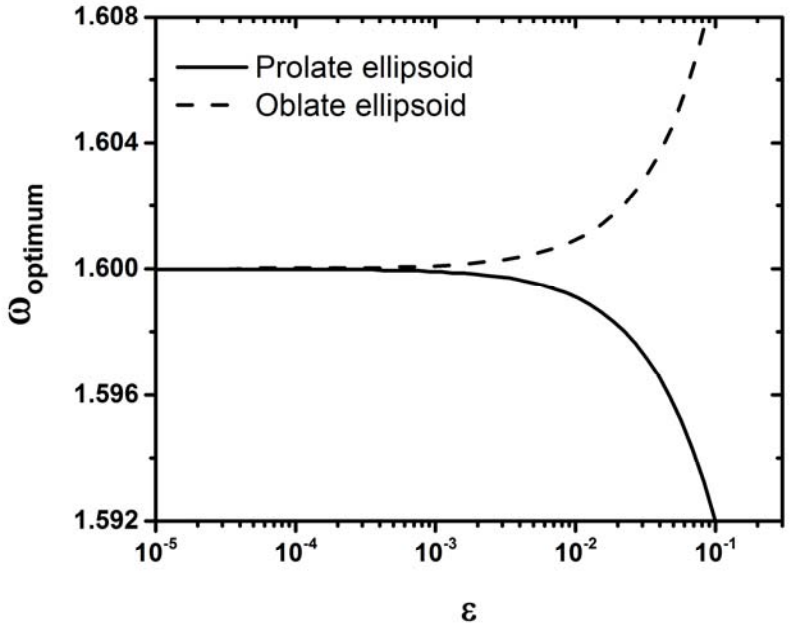

FIGURE B1. The optimum value of the exponent appearing in Knud Thomsen's formula (Eq. (40)) as a function of deviation from sphericity characterized by ε.

Second, we provide additional evidence that a value of $\omega = 8/5$ also leads to an accurate estimate of the surface area, typically within 1% error, even for highly deformed shapes. In Table B1, the predicted surface area for $\omega = 1$ and $\omega = 8/5$ is compared against exact calculations for the surface of ellipsoids obtained from the literature (Keller 1979). As we can see there for $\omega = 8/5$, the predictions are all very good resulting in less than 1% error. In contrast, adopting a different value say $\omega = 1$ can result in significant error especially in the third case.

Ellipsoid dimensions	Exact calculation	Eq. (40) with $\omega = 8/5$	Eq. (40) with $\omega = 1.0$
$a=1, b=1, c=0.5$	8.671882703	8.682895169	8.37758041
$a=1, b=0.8, c=0.625$	8.151618924	8.152577417	8.063421144
$a=2, b=1, c=0.25$	13.69921081	13.78079266	11.51917306

TABLE B1. Comparison of predictions surface area (S_D) of Eq. (40) with $R=\sqrt[3]{3V/(4\pi)}=\sqrt[3]{abc}$ and $\lambda_1=(a/R)^2$, $\lambda_2=(b/R)^2$ and $\lambda_3=(c/R)^2$ to exact calculations to 10 significant digits from Keller (2014) for ellipsoids, each with same volume V where $V=4\pi abc/3$.

In addition, in Fig. B2, the variation of the calculation error as a function of ω indicates the minimum calculated error for the three ellipsoids considered in Table 2. This provides further justification for adopting the value of $\omega=8/5$ as the error remains close to the minimum for all the cases considered here.

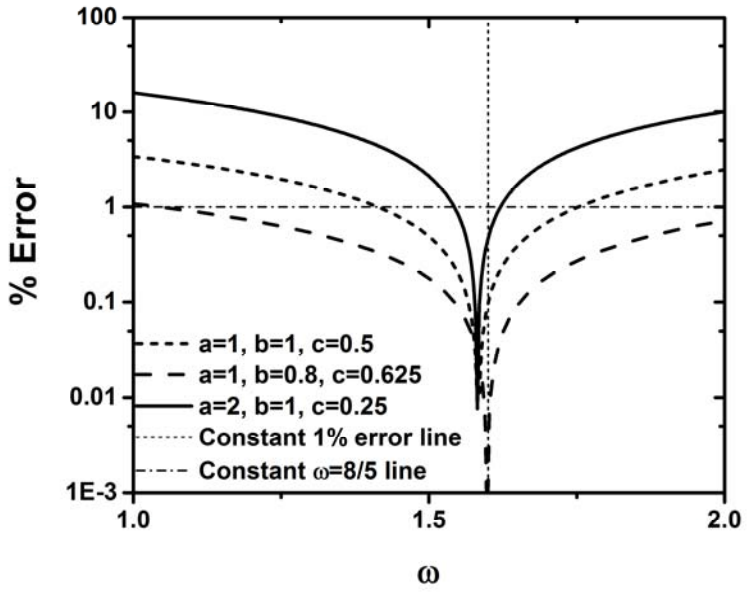

FIGURE B2. The relationship between % error from exact calculations (see table B1) and the value of ω entering Eq. (40). Note that for $\omega=8/5$ denoted by the vertical line, the % error in all the calculations is less than 1%.

Appendix C

This appendix describes the derivations of the derivatives of the dimensionless surface area with respect to the invariants. The starting point is Knud Thomsen's formula, Eq. (40), as

$$h=\left(\frac{\lambda_1^{\omega/2}\lambda_2^{\omega/2}+\lambda_2^{\omega/2}\lambda_3^{\omega/2}+\lambda_3^{\omega/2}\lambda_1^{\omega/2}}{3}\right)^{\frac{1}{\omega}} . \qquad \text{(C 1)}$$

The connection between the partial derivatives of h with respect to the eigenvalues (λ_1, λ_2 and λ_3) and the invariants (I_1, I_2 and I_3) is given by the following relationship

$$\begin{bmatrix} \partial h/\partial \lambda_1 \\ \partial h/\partial \lambda_2 \\ \partial h/\partial \lambda_3 \end{bmatrix} = \begin{bmatrix} \partial I_1/\partial \lambda_1 & \partial I_2/\partial \lambda_1 & \partial I_3/\partial \lambda_1 \\ \partial I_1/\partial \lambda_2 & \partial I_2/\partial \lambda_2 & \partial I_3/\partial \lambda_2 \\ \partial I_1/\partial \lambda_3 & \partial I_2/\partial \lambda_3 & \partial I_3/\partial \lambda_3 \end{bmatrix} \begin{bmatrix} \partial h/\partial I_1 \\ \partial h/\partial I_2 \\ \partial h/\partial I_3 \end{bmatrix}. \tag{C 2}$$

The matrix in this expression can be easily evaluated from the definitions of the invariants, $I_1 = \left(\lambda_1 + \lambda_2 + \lambda_3\right)$, $I_2 = \left(\lambda_1\lambda_2 + \lambda_2\lambda_3 + \lambda_1\lambda_3\right)$ and $I_3 = \lambda_1\lambda_2\lambda_3 = 1$, as

$$\Lambda \equiv \begin{bmatrix} \partial I_1/\partial \lambda_1 & \partial I_2/\partial \lambda_1 & \partial I_3/\partial \lambda_1 \\ \partial I_1/\partial \lambda_2 & \partial I_2/\partial \lambda_2 & \partial I_3/\partial \lambda_2 \\ \partial I_1/\partial \lambda_3 & \partial I_2/\partial \lambda_3 & \partial I_3/\partial \lambda_3 \end{bmatrix} = \begin{bmatrix} 1 & \lambda_2 + \lambda_3 & \lambda_2\lambda_3 \\ 1 & \lambda_1 + \lambda_3 & \lambda_1\lambda_3 \\ 1 & \lambda_1 + \lambda_2 & \lambda_1\lambda_2 \end{bmatrix}, \tag{C 3}$$

resulting to the inverse

$$\Lambda^{-1} = \frac{1}{\left(\lambda_1^2\lambda_2 - \lambda_1\lambda_2^2 - \lambda_1^2\lambda_3 + \lambda_2^2\lambda_3 + \lambda_1\lambda_3^2 - \lambda_2\lambda_3^2\right)} \begin{bmatrix} \lambda_1^2\left(\lambda_2 - \lambda_3\right) & \lambda_2^2\left(\lambda_3 - \lambda_1\right) & \lambda_3^2\left(\lambda_1 - \lambda_2\right) \\ \lambda_1\left(\lambda_3 - \lambda_2\right) & \lambda_2\left(\lambda_1 - \lambda_3\right) & \lambda_3\left(\lambda_2 - \lambda_1\right) \\ \left(\lambda_2 - \lambda_3\right) & \left(\lambda_3 - \lambda_1\right) & \left(\lambda_1 - \lambda_2\right) \end{bmatrix}. \tag{C 4}$$

In addition, from Eq. (C 1), we have

$$\begin{bmatrix} \partial h/\partial \lambda_1 \\ \partial h/\partial \lambda_2 \\ \partial h/\partial \lambda_3 \end{bmatrix} = \frac{3^{-\frac{1}{\omega}}}{2}\left(\lambda_1^{\omega/2}\lambda_2^{\omega/2} + \lambda_2^{\omega/2}\lambda_3^{\omega/2} + \lambda_3^{\omega/2}\lambda_1^{\omega/2}\right)^{\frac{1}{\omega}-1} \begin{bmatrix} \left(\lambda_1^{\omega/2}\lambda_2^{\omega/2} + \lambda_1^{\omega/2}\lambda_3^{\omega/2}\right)\lambda_1^{-1} \\ \left(\lambda_1^{\omega/2}\lambda_2^{\omega/2} + \lambda_2^{\omega/2}\lambda_3^{\omega/2}\right)\lambda_2^{-1} \\ \left(\lambda_2^{\omega/2}\lambda_3^{\omega/2} + \lambda_1^{\omega/2}\lambda_3^{\omega/2}\right)\lambda_3^{-1} \end{bmatrix}. \tag{C 5}$$

Introducing Eq. (C 5) into (C 2), inverting the matrix using Eq. (C 4) and simplifying using the unit determinant constraint, $I_3 = \lambda_1\lambda_2\lambda_3 = 1$, leads to

$$\partial h/\partial I_1 = \frac{3^{-\frac{1}{\omega}}\left(\lambda_1^{\omega/2}\lambda_2^{\omega/2} + \lambda_2^{\omega/2}\lambda_3^{\omega/2} + \lambda_3^{\omega/2}\lambda_1^{\omega/2}\right)^{\frac{1}{\omega}-1}}{2\left(\lambda_1^2\lambda_2 - \lambda_1\lambda_2^2 - \lambda_1^2\lambda_3 + \lambda_2^2\lambda_3 + \lambda_1\lambda_3^2 - \lambda_2\lambda_3^2\right)}\left(\left(\lambda_1\lambda_2\right)^{\frac{\omega}{2}-1}\left(\lambda_2 - \lambda_1\right) + \left(\lambda_2\lambda_3\right)^{\frac{\omega}{2}-1}\left(\lambda_3 - \lambda_2\right) + \left(\lambda_1\lambda_3\right)^{\frac{\omega}{2}-1}\left(\lambda_1 - \lambda_3\right)\right)$$

, (C 6)

and

$$\partial h/\partial I_2 = \frac{3^{-\frac{1}{\omega}}\left(\lambda_1^{\omega/2}\lambda_2^{\omega/2}+\lambda_2^{\omega/2}\lambda_3^{\omega/2}+\lambda_3^{\omega/2}\lambda_1^{\omega/2}\right)^{\frac{1}{\omega}-1}}{2\left(\lambda_1^2\lambda_2-\lambda_1\lambda_2^2-\lambda_1^2\lambda_3+\lambda_2^2\lambda_3+\lambda_1\lambda_3^2-\lambda_2\lambda_3^2\right)}\left((\lambda_1\lambda_2)^{\frac{\omega}{2}}(\lambda_1-\lambda_2)+(\lambda_2\lambda_3)^{\frac{\omega}{2}}(\lambda_2-\lambda_3)+(\lambda_1\lambda_3)^{\frac{\omega}{2}}(\lambda_3-\lambda_1)\right)$$

. (C 7)

The above expressions may be evaluated numerically when computing the relaxation terms of the evolution equation for the conformation tensor. However, for the asymptotic behavior of these function required to evaluate Eq. (50) in the main paper, we consider a similar expansion in terms of τ_C as

$$\lambda_k = 1+\tau_C\lambda_{1k}+\frac{\tau_C^2}{2}\lambda_{2k}+O(\tau_C^3)\ , \tag{C 8}$$

and find that

$$A_1 \equiv \partial h/\partial I_1\big|_{\tau_C=0} = \frac{\omega}{48}(2-\omega) \quad \text{and} \quad A_2 \equiv \partial h/\partial I_2\big|_{\tau_C=0} = \frac{\omega}{48}(2+\omega)\ . \tag{C 9}$$

Appendix D

This appendix shows how the asymptotic behavior at small deformations can be used to determine the macroscopic model parameters. Following Maffettone & Minale (1998), for small deviations to the sphericity of an emulsion droplet induced by flow, one can expand the conformation tensor as

$$C_{\alpha\beta} = \delta_{\alpha\beta}+\tau_C C_{1,\alpha\beta}+O(\tau_C^2) \tag{D 1}$$

where $C_{1,\alpha\beta}$ is a traceless tensor (already shown in Eq. (49)). The evolution equation for the traceless $C_{1,\alpha\beta}$ contribution is readily obtained from Eq. (46) as

$$\tau_C\frac{\partial C_{1,\alpha\beta}}{\partial t} = 2(1-\xi)D_{\alpha\beta}-(a_1+a_2+a_3)(A_1+A_2)C_{1,\alpha\beta}\ , \tag{D 2}$$

The equation for the surface of a drop with a system of axes moving with the center of the particle can be represented by (Barthes-Biesel & Acrivos 1973)

$$r = 1+\varepsilon f(n_l) = 1+3\varepsilon F_{lm}n_l n_m+\varepsilon^2\left[-\frac{6}{5}F_{lm}F_{lm}+105F_{lmpq}n_l n_m n_p n_q\right]+O(\varepsilon^3) \tag{D 3}$$

with $f(n_l)$ a spherical harmonic, $\tau_C=\varepsilon$, $n_l = x_l/r$ with $(n_l n_l)^{1/2}=1$, $r\equiv(x_l x_l)^{1/2}$ and x_l the position vector made dimensionless by the equilibrium drop radius a. Note that F_{lm} must be traceless to satisfy volume

conservation up to first order in ε. The evolution equation for a traceless tensor $F_{\alpha\beta}$ describing the deviations from sphericity, to first order ('$O(\varepsilon)$ theory') has been previously been described by Barthes-Biesel & Acrivos (1973). From these results, the '$O(1)$' Taylor theory simply corresponds to (Rallison 1981)

$$\varepsilon \frac{\partial F_{\alpha\beta}}{\partial t} = \alpha_0 D_{\alpha\beta} - \alpha_1 F_{\alpha\beta} + O(\varepsilon) \ , \tag{D 4}$$

where we have (Barthes-Biesel and Acrivos 1973)

$$\alpha_0 = \frac{5}{3\left(2\lambda+3\right)}, \tag{D 5}$$

$$\alpha_1 = \frac{40\left(\lambda+1\right)}{\left(19\lambda+16\right)\left(2\lambda+3\right)} \ , \tag{D 6}$$

and

$$\varepsilon \ = \ \frac{\mu R}{\gamma} \ \left[=\right] s \ . \tag{D 7}$$

The parameters ξ and the product $\left(a_1+a_2+a_3\right)\left(A_1+A_2\right)$ can therefore be determined by comparing Eqs. (D 2) and (D 4), after determining the relationship between the respective variables in these equations. By combining Eqs. (59), (D 1) and (D 3) and matching terms and considering only the relevant terms to first order in ε, we have

$$\left(1+3\varepsilon F_{lm} n_l n_m\right)^2 \left(\delta_{ij} + \tau_C \hat{C}_{1,ij}\right) n_i n_j = 1, \tag{D 8}$$

where we expand C_{ij}^{-1} as $\left(\delta_{ij} + \tau_C \hat{C}_{1,ij}\right)$. Since $\tau_C = \varepsilon$, we can combine terms at various orders. The zeroth order term is given by

$$\delta_{\alpha\beta} n_\alpha n_\beta = 1 \ , \tag{D 9}$$

and at first order

$$6F_{lm} n_l n_m + \hat{C}_{1,ij} n_i n_j = 0 . \tag{D 10}$$

Consequently, $\hat{C}_{1,ij} = -6F_{ij}$. Finally, we know that $C_{1,ik}C_{kj}^{-1} = \delta_{ij}$, and if we consider the expansion $C_{ij} = \left(\delta_{ij} + \tau_C C_{1,ij}\right)$, together with the result $C_{ij}^{-1} = \left(\delta_{ij} + \tau_C \hat{C}_{1,ij}\right) = \left(\delta_{ij} - 6\tau_C F_{ij}\right)$ we end up with the relationship

$$C_{1,ij} = 6F_{ij} \ , \tag{D 11}$$

and therefore the relationship between $C_{ij} = \left(\delta_{ij} + \tau_C C_{1,ij}\right)$ and $C_{ij}^{-1} = \left(\delta_{ij} + \tau_C \hat{C}_{1,ij}\right)$ satisfies the Woodbury matrix identity (Hager 1989). Finally plugging the result of Eq. (D 11) into Eq. (D 2) and comparing the resultant equation to Eq. (D 4) yields

$$\frac{\left(1-\xi\right)}{3} = \alpha_0 \ , \tag{D 12}$$

and

$$\left(a_1 + a_2 + a_3\right)\left(A_1 + A_2\right) = \alpha_1 \ . \tag{D 13}$$

REFERENCES

AIT-KADI, A., RAMAZANI, A., GRMELA, M. & ZHOU, C. 1999 “Volume preserving” rheological models for polymer melts and solutions using the GENERIC formalism. *J. Rheol.* **43**, 51-72.

ALMUSALLAM, A. S., LARSON, R. G. & SOLOMON, M. J. 2000 A constitutive model for the prediction of ellipsoidal droplet shapes and stresses in immiscible blends. *J. Rheol.* **44**, 1055-1083.

ALMUSALLAM, A. S., LARSON, R. G. & SOLOMON, M. J. 2004 Comprehensive constitutive model for immiscible blends of Newtonian polymers. *J. Rheol.* **48**, 319-348.

BARTHES-BIÈSEL, D. & ACRIVOS, A. 1973 Deformation and burst of a liquid droplet freely suspended in a linear shear field. *J. Fluid Mech.* **61**, 1-22.

BATCHELOR, G. 1970 The stress system in a suspension of force-free particles. *J. Fluid Mech.* **41**, 545-570.

BENTLEY, B. J. & LEAL, L.G. 1986 An experimental investigation of drop deformation and breakup in steady, two-dimensional linear flows. *J. Fluid Mech*. **167** 241-283.

BERIS, A. N. & EDWARDS, B. J. 1994 Thermodynamics of flowing systems with internal microstructure. Oxford University Press, New York.

BEYER, W. H. 1987 CRC Standard Mathematical Tables, 28th ed. CRC Press, Florida.

CHAFFEY, C. E. & BRENNER, H. 1967 A second-order theory for shear deformation of drops. *J. Colloid Interf. Sci.* **24**, 258-269.

CHOI, S. J. & SCHOWALTER, W. R. 1972 Rheological Properties of Nondilute Suspensions of Deformable Particles. *Phys. Fluids* **18**, 420-427.

DELABY, I., MULLER, R. & ERNST, B. 1995 Drop deformation during elongational flow in blends of viscoelastic fluids. Small deformation theory and comparison with experimental results. *Rheol. Acta* **34**, 525-533.

DOI, M. & OHTA, T. 1991 Dynamics and rheology of complex interfaces. I. *J. Chem. Phys.* **95**, 1242-1248.

EDWARDS, B. J. 1998 An analysis of single and double generator thermodynamic formalisms for the macroscopic description of complex fluids. *J. Non-Equil. Thermody*. **23**, 301-333.

EDWARDS, B. J. & DRESLER, M. 2003 A rheological model with constant approximate volume for immiscible blends of ellipsoidal droplets. *Rheol. Acta* **42**, 326-337.

EDWARDS, B. J., BERIS, A. N. & ÖTTINGER, H. C. 1998 An analysis of single and double generator thermodynamic formalisms for complex fluids. II. The microscopic description. *J. Non-Equil. Thermody.* **23**, 334-350.

EDWARDS, B. J., DRESSLER, M., GRMELA, M. & AIT-KADI, A. 2003 Rheological models with microstructural constraints. *Rheol. Acta* **42**, 64-72.

EINSTEIN, A. 1906 A new determination of molecular dimensions. *Ann. Phys.* **19**, 289-306.

EINSTEIN, A. 1911 *Ann. Phys.* **34**, 591 (errata).

FRANKEL, N. A. & ACRIVOS, A. 1970 The constitutive equation for a dilute emulsion. *J. Fluid Mech.* **44**, 65-78.

GORDON, R.J. & SCHOWALTER, W.R. 1972 Anisotropic fluid theory: a different approach to the Dumbbell theory of dilute polymer solutions. *Trans . Soc. Rheol.* **16**, 79-97.

GRMELA, M. 1984. Particle and bracket formulations of kinetic equations. *Contemp. Math*. ***28***, 125-132.

GRMELA, M. 1991 "Mesoscopic dynamics and thermodynamics: Applications to polymeric fluids." In: Rheological modelling: Thermodynamical and statistical approaches, edited by J. Casas-Vazquez and D. Jou, *Lecture Notes in Physics* Vol. 381, 99-125, Springer, Berlin.

GRMELA, M. 1993 Thermodynamics of driven systems. *Phys. Rev. E* **48**, 919-930.

GRMELA, M. & AIT-KADI, A. 1998 Rheology of inhomogeneous immiscible blends. *J. Non-Newtonian Fluid. Mech.* **77**, 191-199.

GRMELA, M & ÖTTINGER, H. C. 1997 Dynamics and thermodynamics of complex fluids. I. Development of a general formalism. *Phys. Rev. E.* **56**, 6620–6632.

GRMELA, M., AIT-KADI, A. & UTRACKI, L. A. 1998 Blends of two immiscible and rheologically different fluids. *J. Non-Newtonian Fluid. Mech.* **77**, 253-259.
GRMELA, M., BOUSMINA, M. & PALIERNE, J. M. 2001 On the rheology of immiscible blends. *Rheol. Acta* **40**, 560-569.
GRMELA, M., AMMAR, A., CHINESTA, F. & MAÎTREJEAN, G. 2014 A mesoscopic rheological model of moderately concentrated colloids. *J. Non-Newtonian Fluid. Mech.* **212**, 1-12.
GUENTHER, G. K. & BAIRD, D. G. 1996 An evaluation of the Doi–Ohta theory for an immiscible polymer blend. *J. Rheol.* **40**, 1-20.
GUIDO, S. & VILLONE, M. 1998 Three-dimensional shape of a drop under simple shear flow. *J. Rheol.* **42**, 395-415.
GUIDO, S., MINALE, M. & MAFFETTONE, P. L. 2000 Drop shape dynamics under shear-flow reversal. *J. Rheol.* **44**, 1385-1399.
HAGER, W. W. 1989 Updating the inverse of a matrix. *SIAM review* **31**(2), 221-239.
HAND, G.L. 1962 A theory of anisotropic fluids. *J. Fluid Mech.* 13 33–46
HAPPEL, J. & BRENNER, H. 1983 Low Reynolds number hydrodynamics: with special applications to particulate media Vol. 1, Springer, Berlin.
JACKSON, N. E. & TUCKER III, C. L. 2003 A model for large deformation of an ellipsoidal droplet with interfacial tension. *J. Rheol.* **47**, 659-682.
JAUMANN, G. 1911 Geschlossenes System physikalischer und chemischer Differentialgesetze. *Sitzungsberichte Akad. Wiss. Wien IIa* **120**, 385-530.
KELLER, S.R. 1979 On the surface area of the ellipsoid. *Math. Comput.* **33**, 310-314.
KENNEDY, M.R., POZRIKIDIS, C. & SKALAK, R. 1994. Motion and deformation of liquid drops, and the rheology of dilute emulsions in simple shear flow. *Computers & Fluids*, **23**, 251-278.
LEE, H. M. & PARK, O. O. 1994 Rheology and dynamics of immiscible polymer blends. *J. Rheol.* **38**, 1405-1425.
LOEWENBERG, M. & HINCH, E. J. 1996 Numerical simulation of a concentrated emulsion in shear flow. *J. Fluid Mech.* **321**, 395-419.
MAFFETTONE, P. & MINALE, M. 1998 Equation of change for ellipsoidal drops in viscous flow. *J. Non-Newtonian Fluid. Mech.* **78,** 227-241.
MINALE, M. 2004 Deformation of a non-Newtonian ellipsoidal drop in a non-Newtonian matrix: extension of Maffettone–Minale model. *J. Non-Newtonian Fluid. Mech.* **123**, 151-160.
MINALE, M. 2010 Models for the deformation of a single ellipsoidal drop: a review. *Rheol. Acta* **49**, 789-806.
MWASAME, P. M., WAGNER, N. J. & BERIS, A. N. 2017 Micro-inertia effects in material flow. *Phys. Rev. Lett.* (submitted).
OLDROYD, J. G. 1953 The elastic and viscous properties of emulsions and suspensions. *Proc. Roy. Soc. Lond. A* **218**, 122-132.
ÖTTINGER, H. C. & GRMELA, M. 1997 Dynamics and thermodynamics of complex fluids. II. Illustrations of a general formalism. *Phys. Rev. E.* **56,** 6633–6655.
PALIERNE, J. F. 1990 Linear rheology of viscoelastic emulsions with interfacial tension. *Rheol. Acta* **29**, 204-214.
RAJA, R. V., SUBRAMANIAN ,G. & KOCH, D. L. 2010 Inertial effects on the rheology of a dilute emulsion. *J. Fluid Mech.* **646**, 255-296.
RALLISON, J. M. 1980 Note on the time-dependent deformation of a viscous drop which is almost spherical. *J. Fluid Mech.* **98**, 625-633.
RALLISON, J. M. 1984 The deformation of small viscous drops and bubbles in shear flows. *Annu. Rev. Fluid Mech.* **16**, 45-66.

RALLISON, J. M. & ACRIVOS, A. 1978 A numerical study of the deformation and burst of a viscous drop in an extensional flow. *J. Fluid Mech.* **89**, 191-200.
SCHOWALTER, W. R., CHAFFEY, C. E. & BRENNER, H. 1968 Rheological behavior of a dilute emulsion. *J. Colloid Interf. Sci.* **26**, 152-160.
STONE, H. W. 1994 Dynamics of drop deformation and breakup in viscous fluids. The viscosity of a fluid containing small drops of another fluid. *Ann. Rev. Fluid Mech.* **26**, 65-102.
TAKAHASHI, Y., KURASHIMA, N., NODA, I. & DOI, M. 1994 Experimental tests of the scaling relation for textured materials in mixtures of two immiscible fluids. *J. Rheol.* **38**, 699-712.
TAYLOR, G. I. 1932 The viscosity of a fluid containing small drops of another fluid, *Proc. Roy. Soc. Lond. A* **138***,* 41-48.
TAYLOR, G. I. 1934 The formation of emulsions in definable fields of flow. *Proc. Roy. Soc. Lond. A* **146**, 501-523.
TORZA, S., COX, R. & MASON, S. G. 1972 Particle motions in sheared suspensions XXVII. Transient and steady deformation and burst of liquid drops. *J. Colloid Interf. Sci.* **38**, 395-411.
VERMANT, J., VAN PUYVELDE, P., MOLDENAERS, P., MEWIS, J. & FULLER, G. G. 1998 Anisotropy and orientation of the microstructure in viscous emulsions during shear flow. *Langmuir* **14**, 1612-1617.
WAGNER, N. J., ÖTTINGER, H. C. & EDWARDS, B. J. 1999 Generalized Doi–Ohta model for multiphase flow developed via GENERIC. *AIChE J.* **45**, 1169-1181.
VINCKIER, I., MOLDENAERS, P. & MEWIS, J. 1996 Relationship between rheology and morphology of model blends in steady shear flow. *J. Rheol.* **40**, 613-631.
VINCKIER, I., MEWIS, J. & MOLDENAERS, P. 1997 Stress relaxation as a microstructural probe for immiscible polymer blends. *Rheol. Acta* **36**, 513-523.
WETZEL, E. D. & TUCKER III, C. L. 1999 Area tensors for modeling microstructure during laminar liquid-liquid mixing. *Int. J. Multiphase Flow* **25**, 35-61.
WETZEL, E. D. & TUCKER III, C. L. 2001 Droplet deformation in dispersions with unequal viscosities and zero interfacial tension. *J. Fluid Mech.* **426**, 199-228.
XU, D., CUI, J., BANSAL, R., HAO, X., LIU, J., CHEN, W. & PETERSON, B. S. 2009 The ellipsoidal area ratio: an alternative anisotropy index for diffusion tensor imaging. *Magn. Reson. Imaging* ***27***(3), 311-323.
YU, W. & BOUSIMA, M. 2003 Ellipsoidal model for droplet deformation in emulsions. *J. Rheol.* **47**, 1011-1039.
YU, W. & ZHOU, C. 2007 A simple constitutive equation for immiscible blends. *J. Rheol.* **51**, 179-194.